INFLUENCE OF DIFFUSION IN TISSUE ENGINEERING BIOREACTORS

By

DHANANJAY V. DHANE

Bachelor of Science in Petrochemical Engineering

University of Pune

Pune, Maharashtra, India

2005

Submitted to the Faculty of the
Graduate College of the
Oklahoma State University
in partial fulfillment of
the requirements for
the Degree of
MASTER OF SCIENCE
December, 2010

INFLUENCE OF DIFFUSION IN TISSUE

ENGINEERING BIOREACTORS

Thesis Approved:

Dr. Sundar Madihally

Thesis Adviser

Dr. Gary Foutch

Dr. A. J. Johannes

Dr. Mark E. Payton

Dean of the Graduate College

.

ACKNOWLEDGMENTS

First and foremost, I am thankful to my father, *Late Mr. Vishnu P. Dhane,* for having faith in me and helping me reach this point in my life. It is due to his efforts and immense sacrifice that I have been fortunate enough to get quality education. I extend my gratitude and a special thanks to my elder brother *Abhijit* for his continuous encouragement and guidance.

I would like to thank from bottom of my heart *Dr. Sundar Madihally,* my thesis advisor, who gave me an opportunity to pursue my master's research under his valuable guidance. He has been so considerate and supportive of my work and provided ideas throughout my thesis work. His valuable guidance, patience, knowledge, time, charm and faith made this work possible. I so appreciate your time in reviewing my work and making corrections.

I would also like to thank *Dr. Gary Foutch* and *Dr. A. J. Johannes* for believing in me and accepting to be a committee member in my master's program. They provided some valuable inputs and suggestions. I thank you for your valuable time in reviewing my thesis and help me improve, refine and expand my thesis.

I would like to thank my colleagues *Paul* and *Mamatha* for giving their valued inputs when needed. I appreciate the moral support they provided during my project work. Besides the names mentioned above, I would like to thank my friends *Hrishikesh,*

Gaurav, Kumar, Manish, Swapnil and *Shalaka* for their emotional support over the last two and half years.

Last but not the least; I owe my deepest and sincere gratitude towards *Oklahoma State University* for giving me a chance to work with such great facilities and amenities. Without the support of *OSU*, the projects I worked on would have been a distant reality.

TABLE OF CONTENTS

LIST OF TABLES

Table Page

LIST OF FIGURES

Figure Page

Figure Page

CHAPTER I

INTRODUCTION

Tissue Engineering is an interdisciplinary field involving life sciences and engineering dealing with regenerating tissues and organs to replace or support the function of defective body parts for the betterment of humankind. According to Organ Procurement Transplantation Network (OPTN) the number of patients waiting for organ transplant as of November 2010 was 109971 whereas the number of transplants that occurred in period January - August 2010 was only 19249. This difference between demand and supply has created the need for Tissue Engineering.

Fabrication of tissues in the laboratory environment requires engineering of scaffolds, cells and biologically active molecules (biofactor) like proteins, peptides and carbohydrates. *Scaffolds* are three dimensional synthetic frame structures which serve as a mimic of extracellular matrix for cell adhesion, migration and proliferation. A successful scaffold must meet the balance between mechanical function and biofactor delivery while providing sequential transition in which the regenerated tissue assumes functions as the scaffold degrades (Hollister 2005). The scaffold should be biocompatible and promote growth and cell adhesion. While the cells generate their own natural matrix elements, the synthetic matrix should degrade into non-toxic components, which can be eliminated from the body (Freyman et al. 2001).

Natural polymers such as chitosan, gelatin, fibrins, gluten and synthetic polymers such as polyvinyl alcohol (PVA), polylactic acid (PLLA), polyglycolic acid (PGA), poly (lactide-co-glycolide) (PLGA) are used in scaffold preparation. The interest in natural polymers was generated due to their biocompatibility, availability and ease of processing. However, natural polymers suffer from problems like cross contamination, batch to batch variations and high price (Mark Saltzman and Baldwin 1998). Hence, the reproducibility of scaffold characteristics with natural polymers, such as mechanical strength, is of a concern. On the other hand, synthetic polymers can be manufactured by aiming at specific properties, like mechanical property, surface morphology, porosity, without encountering major obstacles. However, the disadvantage of synthetic polymers is the lack of cell recognition signals (Kim and Mooney 1998). Designing and development of scaffolds from different materials has been studied extensively (Yang et al. 2001; Courtney et al. 2006; Liu et al. 2007; Cheng et al. 2008). Also, generating natural scaffolds from different tissues after removing cells are explored. For example, scientists have developed scaffolds from the liver by removing the cells and retaining the extracellular matrix and vascular channels (Uygun et al. 2010).

Tissue engineering can be performed via two approaches namely *in situ* and *in vitro*. *In situ* technique utilizes natural healing mechanism by implanting the scaffolds without cells inside the body and relying on migration of cells from the neighboring tissues on to the scaffold. In contrast *in vitro* technique utilizes cell culture conditions by seeding cells on to the scaffold outside the body and allowing the cells to establish cell-composite grafts followed by *in vivo* implantation of the grafts. This process has to be executed aseptically under physiological temperature, pH with sufficient amount of

nutrients. Since a significant number of cells are required to colonize 3D porous structures in seeded technique, bioreactors are utilized as a way to distribute the nutrients within the biodegradable porous structures.

Bioreactors of different configurations and flow systems have been utilized for regenerating tissues in seeded technique (Martin et al. 2004; Martin and Vermette 2005; Cummings and Waters 2007). Some studies have shown an improvement in the quality of the regenerated tissue (Niklason et al. 1999). However, other studies have shown deterioration in the quality of the tissue (Heydarkhan-Hagvall et al. 2006). The mechanical stimulus needed by the cell for accelerated growth is provided by the fluid flow inside the reactor (Powell et al. 2002; Vance et al. 2005). Fundamental concepts in developing these reactors are not well defined. For example, many tissues such as skin, bladder, and cartilage have a high aspect ratio (large surface area relative to the thickness). In these systems, one has to understand the fluid distribution and the effect of shape of the reactor (Heydarkhan-Hagvall et al. 2006), as non-uniform flow patterns within the reactor lead to poor quality of regenerated tissues via multiple modes, i) poor distribution of nutrients, and ii) non-uniform shear stress distribution, which affects the structure as well as the assembly of extracellular matrix (ECM) elements. Further, tissue regeneration is a dynamic process where the porous characteristics change due to cell growth, newly deposited matrix components, and degradation of the porous architecture. These changes affect the transport characteristics.

To better understand the effect of fluid flow in bioreactors, few studies are performed using computational fluid dynamics tools in high aspect ratio bioreactors. One of the previous studies suggested the possibility of using (Devarapalli et al. 2009) a

circular shape parallel plate flow-through reactor for uniform nutrient distribution. Nutrient consumption patterns were studied for various cells types along with flow pattern and residence time distribution analysis.

Although these designs showed some advantages, they have certain drawbacks. Since the fluid is flowing through the porous structure, maximum allowable flow rate is restricted by the mechanical characteristics of the porous structure. High flow rates necessary during healing could damage the regenerating tissue. Further, flow rate through the scaffold microarchitecture dictates the local shear stresses to which cells are exposed to. High shear rates could be detrimental to the cells and to the assembly of newly synthesized matrix elements. Hence, there is a need to evaluate alternative configurations for this design.

In this study, alternatives to the circular reactor shape design are evaluated along with varying thickness of the porous structures. Then the effects of changing porous characteristics during tissue regeneration, attributed to *de novo* synthesis of matrix elements and cell colonization, are also evaluated. The two specific aims of this study are:

***Specific Aim 1*: To determine alternate design for a flow through bioreactor.**

Two new designs of split flow parallel plate reactor were considered. The simulation was carried out using COMSOL Multiphysics 3.5a (COMSOL, Inc., Burlington, MA). The flow of the system was analyzed by using Navier-Stokes equations in non-porous region of the reactor and Brinkman equations in the porous region of the reactor. The steady state momentum transport was utilized in the convective diffusion equation to obtain the concentration profiles. Metabolic

consumption of oxygen and glucose was included using Michaelis-Menten kinetic rate laws. Along with differential pressure, shear tress distribution inside the bioreactor was analyzed. *Péclet* number was calculated at various locations inside the bioreactor for determination of flow regime. It was observed that the nutrient distribution inside the scaffold occurs only due to diffusion as the scaffold is placed at a lower level and nutrients flow over it.

Specific Aim 2: To assess the effect of diffusivity changes on nutrient transport.

Previous simulations were performed under constant diffusivity which may not be a factor when nutrient distribution is primarily by convective flow i.e., when *Péclet* number is very high. However, when the nutrient distribution is limited by diffusion, understanding the changes in diffusivity during regenerative process is important. Experiments were conducted to assess the diffusivity of glucose through chitosan-gelatin porous scaffolds of three different compositions using a custom-built apparatus (explained in chapter III) that accommodated4 cm × 4 cm sample. Since the values of diffusivity were determined to be a magnitude higher than infinite diffusivity, the effective diffusion coefficient of nutrients through the porous scaffold was calculated using Mackie-Meares equation. These values were incorporated in the reactor simulation using COMSOL Multiphysics 3.5a. To find out the maximum scaffold thickness that could be fed using diffusive flow, further studies were performed by changing scaffold thicknesses. Based on the results of concentration profiles of nutrients within the scaffold, the reactor was reconfigured with an extra inlet and outlet and with an extra channel to reduce the distance through which the nutrients had to diffuse. Further, to

reduce the ‘Hold-up’ volume of the reactor, the design was reconfigured by reducing the channel thickness. This modified design was checked for varying thicknesses of scaffold. The comparison of minimum oxygen concentration, pressure drop and shear stress value indicated that the modified design gives higher values of minimum oxygen concentration for the same ‘hold-up’ volume as compared to the first design which had only one parallel channel.

CHAPTER II

LITERATURE REVIEW

2.1 TISSUE ENGINEERING

Tissue engineering has gained the importance because of the large gap between the organ acceptors and organ donors. Tissue engineering offers the advantage of providing the functionally replaceable tissues widely and economically. The general methodology of tissue engineering is based on two basic techniques,

a) *in situ* regeneration of tissue

b) Implantation of *in vitro* regenerated tissue

With the *in situ* technique, a scaffold is implanted directly into the human body and the cells are allowed to grow naturally and carry out the healing procedure or cells are injected onto the scaffold and are allowed to multiply inside the human body. There is much interest in the *in situ* growth of tissue from injected cells where mechanical stresses are applied naturally. Blood vessels with superior mechanical properties have been grown *in situ* in an animal model using a natural scaffold that recruited endothelial cells (Griffith and Naughton 2002). However, translating vascular successes in animals

to humans is difficult because human and animal endothelia behave very differently (Griffith and Naughton 2002).

With the *in vitro* technique, the tissue is regenerated inside the glass. The cells seeded on a scaffold are allowed to take the form of the scaffold. The matured tissue is then implanted into the body **(Figure 2.1)**. With *in vitro* tissue engineering technique, tissue can be manipulated according to the requirement of the tissue to be grown and thus increases the chances of improvement of cellular binding.

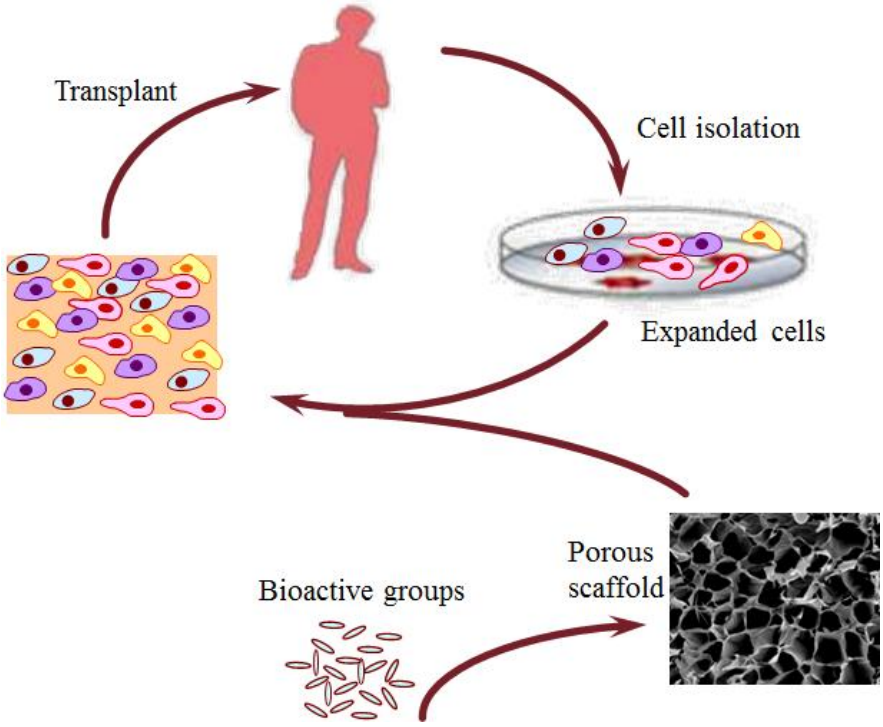

Figure 2.1: Schematic of *in-vitro* Tissue Engineering

2.2 POROUS SCAFFOLDS:

Materials which are biocompatible and can be transplanted in the body to replace or repair faulty organ or tissue are termed biomaterials. To make biomaterials act as

extracellular matrix (ECM) elements, they are formed into a scaffold. These scaffolds define a three-dimensional space for the formation of new tissues with appropriate structure, and guide the development of new tissues with appropriate function (Griffith and Naughton 2002). While supporting biological activity, the scaffold degrades transiently and allows regeneration of tissue without any reminiscent foreign material (Langer and Vacanti 1993). Some natural and synthetic polymers are used to generate such scaffolds. Natural polymeric gels, such as collagen, alginate, chitosan, gelatin, polycaprolactone (PCL) have been used successfully (Risbud and Sittinger 2002). This study considers chitosan and gelatin as basic biomaterials for production of the scaffold, as they have been studied earlier by our group. Chitosan is a natural polymer derived by deacetylation of chitin, the primary structural element present in exoskeletons of shrimps and crab shells and cell walls of fungi. Chitosan is an inexpensive natural polymeric material which has been used extensively for wound healing and drug delivery purposes (Chou. 2003; Ishihara et al. 2006). Gelatin is a protein produced from bones, connective tissues and organs of animals like cows, horses and pigs. Gelatin has been used previously for preparation of scaffolds (Mao et al. 2003). Some of the various attributes that make gelatin suitable as a biomaterial for tissue engineering are, low cost, good biocompatibility, biodegradability, low immunogenicity, increased cell adhesion, migration, differentiation and proliferation. Gelatin is blended with chitosan to improve its biological activity, as it promotes cell adhesion, migration and forms a polyelectrolyte complex (Huang et al. 2005). The backbone of gelatin has free carboxyl groups, enabling it to blend with cationic chitosan to form a network by hydrogen bonding (Thein-Han et al. 2009).

Preparation of scaffolds: The techniques like fiber melts, fiber bonding, phase separation, solvent casting and particulate leaching (Yang et al. 2001), gas foaming, emulsion freeze drying, electrospinning, three dimensional printing (O'Brien et al. 2004; Hollister 2005; Reignier and Huneault 2006; Weigel et al. 2006) are commonly used for preparation of scaffolds for tissue engineering applications. Every technique has advantages and disadvantages. In this study controlled rate freeze drying and lyophilization technique (CRFLT) was employed for preparation of porous structures from chitosan and gelatin (Madihally and Matthwe 1999; Moshfeghian et al. 2006). As CRFLT is carried out at low temperatures, the denaturation of biomaterials is avoided; also, CRFLT generates open pore architecture.

In controlled rate freezing, a solution of polymer is prepared by dissolving the polymer in suitable solvent. The solution is then frozen below the freezing temperature of solvent for around 6 hours to make sure that the solution solidifies. Next the solidified solution is freeze dried in a lyophilizer. This step allows the solvent to sublime leaving a porous structure behind. Pores are obtained in the region where solvent crystals have solidified. The alignment of crystal depends upon the direction of cooling. Hence, uniform cooling from the surface is necessary to get uniform pores in the porous structure.

Cells respond in a different manner to 3D porous structure than to 2D membranes. Also, the nature of porous structure, i.e. the porosity, pore size, pore number, mechanical properties, affects the cellular binding, cell migration and differentiation (Wake et al. 1994; Van et al. 2002; Otsuki et al. 2006). So, it is important to understand 3D characteristics of porous structure before every study.

Porosity: Cells like high porosity. The porosity and pore interconnectivity play a significant role in cell survival, proliferation, and migration (Lien et al. 2009; Mandal and Kundu 2009). Higher porosity provides large surface area for the cellular interaction and extra cellular matrix regeneration. Also higher porosity helps in better supply of nutrients across the scaffold.

Pore size: Pore size depends upon the technique of scaffold preparation from biomaterial solution and the concentration of the solution. Pore size affects the amount of ECM formation. The extent of ECM secretion also increases with increase in the pore size (Lien et al. 2009). The average pore size of the scaffolds greatly affects the growth and penetration of cells in the 3D structure (Annabi et al. 2010). Small pore size might hinder the nutrient supply, whereas it improves the retention of extra cellular matrix. So, it is important to have an optimal pore size. (Whang et al. 1999) found the optimal pore size for fibroblast in-growth is 5-15µm, for the in-growth of hepatocytes is 20µm, for regeneration of adult mammalian skin is 20-125 µm, and for regeneration of bone 100-350µm. As the cells grow and spread their ECM the pore size decreases.

Topography: The surface characteristic of the scaffold is termed as its topography. This property dictates the cell adhesion and cellular migration. Certain cell types like smooth muscle cells and chondrocytes require high surface roughness whereas some require low surface roughness.

Mechanotransduction: The signals or responses that are generated by the cells during regeneration phase or during working phase to the mechanical stimuli are termed as mechanotransduction. The organs like blood vessels and heart, lungs, urinary bladder,

muscles inside the body are continuously under mechanical stress due to blood flow, air circulation, urine transport and due to weight of the body, respectively. So, it is important to regenerate the tissues in the same conditions as they are exposed inside the body. Certain *in vitro* studies point out that the flow of nutrients through the porous structure would dictate the shear stress inside the micro structure and these shear stresses instigate the signal transduction cascades that lead to altered gene expressions (Papadaki et al. 1999; Chiu et al. 2009). The production of ECMs is also affected by the presence of flow through the scaffold on which the cells are growing. Certain cells types like endothelial cells when growing on the scaffolds align themselves in the direction of the nutrient flow (Gray et al. 1988; Takahashi and Berk 1996). Along with local hydrodynamic stresses, the cells also experience stresses due to contact inhibition and due to increased tissue density.

2.3 BIOREACTORS IN TISSUE ENGINEERING:

Bioreactors are needed to transform the research scale product designs to large scale production of biologically functional tissues that are reproducible, safe and economic (Chen and Hu 2006). Bioreactors have been used to provide nourishment to the growing tissue on the scaffold as well as to provide the cells with the necessary mechanical forces. The *in vitro* cultivation of 3D constructs in the bioreactor that efficiently provides nutrition to the cells, possibly combined with the application of mechanical stimulation to direct the cellular activity, differentiation and function, is an important step towards the development of functional grafts (Chen and Hu 2006).

Bioreactors are well established for the cultivation of microbes or mammalian cells under monitored and controlled environmental and operational conditions (e.g., pH, temperature, oxygen tension, and nutrient supply) up to an industrial scale (Portner et al. 2005). However the concepts of 2D cell culture cannot be applied to 3D tissue regeneration on porous scaffolds. Also, an individualized bioreactor design will be needed for each type of tissue construct due to individualized requirements by the cells. Hence, there is a need to design tissue-specific bioreactors on the basis of comprehensive understanding of biological and engineering aspects. Diffusion limitation, of nutrient mass transfer to the growing cells, has been one of the more important constraints the in bioreactor studies.

Flow systems like rotating vessels, spinner flasks and flow through perfusion systems have been considered for increased proliferation of different cell types (Hoerstrup et al. 2000). In general, cell culture bioreactors have to meet demands like cell to cell contact, surface for cell detachment, homogenous and low shear mixing and aeration, scale-up capability and ease of handling. Some of the bioreactors utilized in tissue engineering are discussed below in brief:

Rotating Shaft Bioreactor (RSB): The bioreactor (**Figure 2.2**) is oriented horizontally and has ports for culture media and gas perfusion which allow for continuous media replenishment and oxygen supply via surface aeration. The half of the space in RSB is filled with media and the shaft is driven by a bidirectional peristaltic pump. The rotation moves the scaffold constructs between gas and liquid phases in an oscillating fashion, thus leading to efficient oxygen and nutrient transfer. Also, when the constructs are moving in the liquid phase, the construct movement relative to the medium

enables easier liquid penetration into the interior, thus enhancing the nutrient transfer and imparting more fluid-induced shear to the interior cells (Chen and Hu 2006).

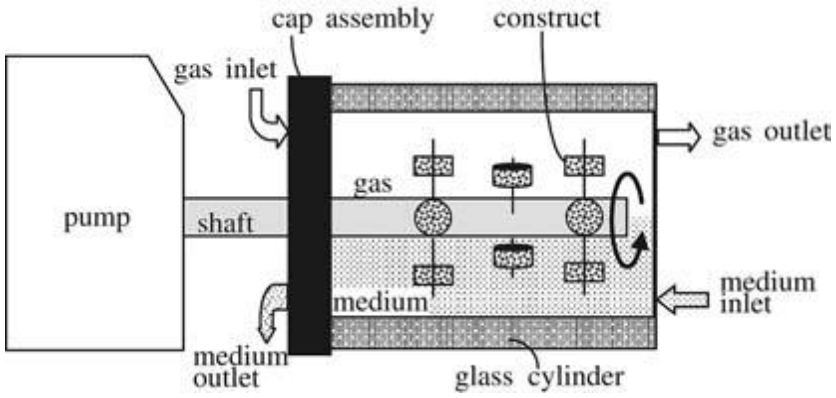

Figure2.2: Rotating Shaft Bioreactor (Chen et al 2006).

Hollow Fiber Bioreactors: A hollow fiber reactor **(Figure 2.3)** consists of a closed vessel filled with culture media and mammalian cells into which a bundle of semi-permeable hollow fibers is inserted. The hollow fibers provide nutrients to the cells and eliminate their wastes, mimicking *in vivo* blood vessels. The main advantage of using such a reactor is to provide nutrients to the center of the growing tissues (Martin and Vermette 2005). This study shows that a large number of hollow fibers are needed to supply sufficient oxygen to obtain a homogeneous cell population. A 1mm thick cartilage tissue has been reported for hollow fiber reactor, which is a marginal improvement as compared to cartilage tissues grown in stirred reactor configurations.

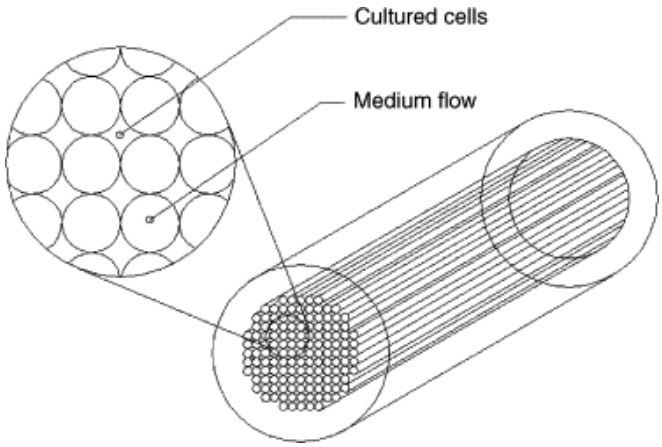

Figure2.3: Hollow Fiber Bioreactor. (Martin et al 2005)

Perfusion Bioreactor: Poor cell growth can be overcome by a perfusion system which is often in conjunction with chambers, columns or cartridges that hold the cell/scaffold constructs. Direct perfusion bioreactors, where medium flows directly through the pores of the scaffold, can be used for seeding and culturing 3D constructs. During seeding, cells are transported directly into the scaffold pores, yielding a highly uniform cell distribution. During culture, medium flowing through the construct enhances the mass transfer not only at the periphery but also within internal pores of the construct (Wendt, Marsano et al. 2003). Problems associated with poor diffusion can be mitigated with a flow perfusion bioreactor in which media is forced through the scaffold pore network (Jaasma, Plunkett et al. 2008). The flow of medium through the scaffold pores benefits cell differentiation by enhancing nutrient transport to the scaffold interior and by providing mechanical stimulation in the form of liquid shear (Holtorf, Sheffield et al. 2005).

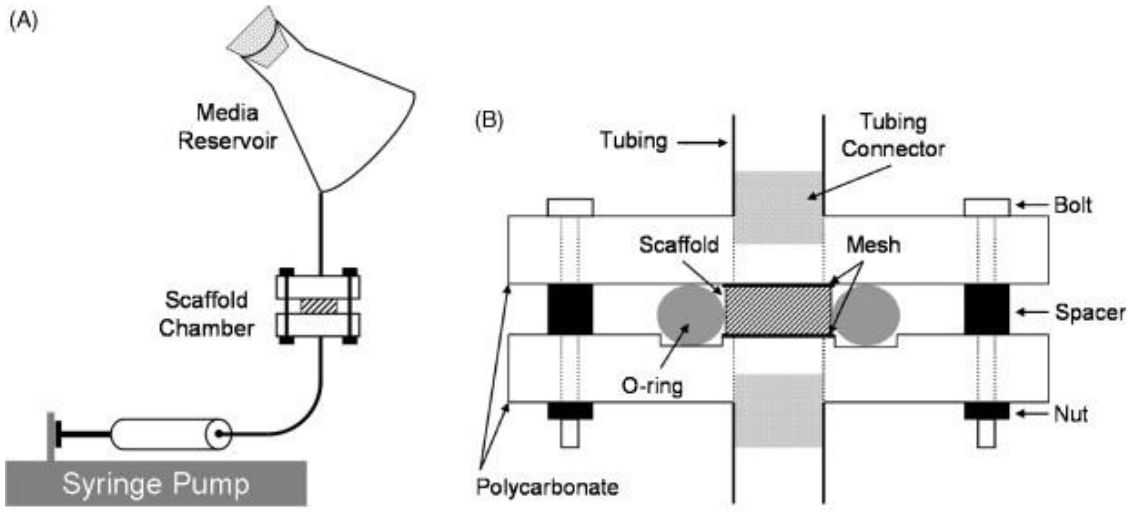

Figure 2.4: Direct perfusion bioreactor. A) bioreactor system. B) cross-section of scaffold chamber. (Jaasma et al 2008).

Parallel plate Bioreactor: Parallel plate bioreactors have been studied (Reich and Frangos 1991; Koller et al. 1993) for observing the effects of flow, to maintain primary cells for cellular therapy and to investigate synthetic function of porcine hepatocytes (Shito et al. 2001). Parallel plate bioreactors have not been studied in detail for culturing 3D tissues having large surface area. In these reactors, the scaffold is subjected to hydraulic forces due to fluid flow and so the cells can experience micromechanical properties of individual fibers and local stresses within the porous structure (Devarapalli 2009). The parallel plate design provides support to the scaffold and growing tissue as well as the circular shape of the reactor helps in eliminating the dead spaces.

2.4 CFD MODELING:

For the purpose of computation fluid dynamic modeling, the geometry of the object to be studied is drawn using CFD software. This geometry is meshed for creating node points at which the equations will be solved. Further, the governing equations of the process taking place in and around the model are integrated in the simulation and the simulation is run to get the results. Computational Fluid dynamics has been used since long in chemical industry to simulate the flow of gases and liquids, movement of aerodynamic bodies, for heat transfer estimations and chemical reactions. The flow of fluid through the bioreactors affects the cell adhesion, cell growth and proliferation and nutrient distribution (Singh and Hutmacher 2009). So, the optimal flow conditions within a bioreactor should not be determined through a trial-and-error approach but rather should be supported by simulation methods (Martin et al. 2004). To understand the influence of shear stresses on 3 D cultures (Porter et al. 2005) and (Raimondi et al. 2006) modeled the effects of perfusion. These studies used Navier-Stokes equations to model the flows without considering the 3D structure. In other studies (Chung et al. 2007) porosity based permeability was used to understand the fluid dynamics in a perfusion system. While, (Boschetti et al. 2006) modeled flow through a 3D scaffold for predicting shear stresses acting on cells as a function of porosity, pore size and medium flow rate. However, all these studies were based on small cylindrical scaffolds and the flow characteristics were analyzed using Darcy's equations. The Brinkman equation accounts for both viscous and drag forces in the porous medium and reduces to either the Navier-Stokes equation or Darcy's law if either of the force becomes dominant (Capuani et al. 2003). In my study, I used Brinkman equation to study the flow dynamics within the

porous structure to mimic the tissue regeneration process. I calculated the permeability based on the pore size keeping the number of pores constant and diffusivity of nutrient based on the porosity of scaffold. However, porous characteristics change during tissue regeneration, i.e., permeability of the matrix decreases due to decrease in pore size.

Tissues, such as skin and bladder, have high surface areas. So, to study tissue specific reactor conditions and to understand the flow dynamics, I designed high aspect ratio parallel plate bioreactors of a diameter of 100 mm and of varied thicknesses to evaluate the design of the bioreactor. The concentration profiles of the nutrients and shear stresses over the porous structure were analyzed and the effect on tissue growth was checked.

CHAPTER III

DETERMINATION OF ALTERNATIVE DESIGN FOR A FLOW THROUGH REACTOR

3.1 Introduction:

In the flow through bioreactors the flow of nutrients has to pass through the entire scaffold. Hence, the nutrient distributions and their sufficiency depend upon the flow rate of the medium carrying through the reactor. Many flow through reactor configurations have been evaluated (Mueller et al. 1999; Bancroft et al. 2003). One such configuration which utilized parallel flow through reactor (referred as Design 6 in the manuscript) had an advantage of uniform flow distribution (Devarapalli et al. 2009) in high-aspect ratio (100 mm diameter and 2 mm thickness) porous structures. However, the maximum allowable flow rate is restricted by the mechanical characteristics of the porous structure in flow through configuration. High flow rates necessary during later stages of healing could damage the regenerating tissue. Further, flow rate through the scaffold micro-architecture dictates the local shear stresses to which cells are exposed to. High shear rates could be detrimental to the cells and to the assembly of newly synthesized matrix elements. Hence, there is a need to find alternative configuration for a flow-through reactor. I evaluated two new designs (Design 7 and Design8) having 'split flow' arrangement while keeping the diameter, porous structure thickness and inlet/outlet shapes constant.

Nutrient transport and consumption was investigated for regeneration of muscles tissue using smooth muscle cells (SMC) using kinetic constants reported in the literature. The pressure drop, velocity and shear stress profiles analysis was done. Further, simulations were performed for understanding the effect of changing pore size on account of proliferation of cells and *de novo* generation of extracellular matrix elements. In addition, the previous study utilized chitosan-based 3D scaffold characteristics (Devarapalli et al. 2009). However, recently it was reported that chitosan structures demonstrated reduced viability and proliferation as they lack the cell binding domain (Iyer 2009). Alternatively, adding gelatin to the chitosan 3D scaffolds improved cell viability and cell function. To incorporate these advances, I evaluated the reactor configuration for chitosan-gelatin porous structures.

3.2 Materials and Methods:

3.2.1 Sources of material

Chitosan with molecular weight >310 kDa and 85% degree of deacetylation, Gelatin Type A (300 bloom) and glacial acetic acid were obtained from Sigma Aldrich Chemical Co (St. Louis, MO). Ethanol (200 proof) was obtained from Aaper Alcohol and Chemical Company (Shelbyville, KY). All other reagents were purchased from Fisher Scientific (Waltham, MA).

3.2.2 Preparation of the scaffold:

Chitosan-gelatin solutions were prepared in 0.1M acetic acid using deionized water. A well of 100mm diameter was prepared on Teflon sheet using silicon glue and 25mL of chitosan-gelatin solution was poured in the well and frozen overnight at -80^0C. The frozen solution was lyophilized overnight (Virtis, Gardiner, NY) to obtain porous scaffolds as shown in **Figure 3.1**.

The scaffolds obtained had thin non-porous layer on top. This layer is termed as 'skinny layer' and it could act as a barrier for the nutrient transport. In case of scaffold made from (0.5%-0.5% wt/v) chitosan gelatin solution, this layer could be peeled off after the scaffold formation.

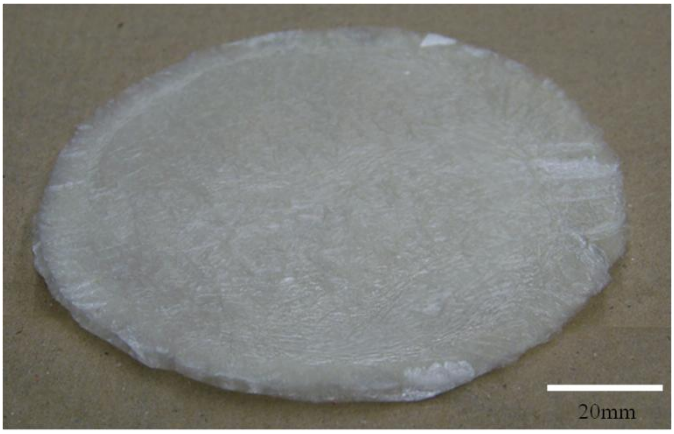

Figure 3.1: Chitosan-Gelatin scaffold.

3.2.3 Porosity and pore size:

Obtained scaffolds were analyzed in dry condition using scanning electron microscope (SEM, Joel JSM 6360) at an accelerating voltage of 10 kV. For this purpose, small sections of dry scaffolds were sputter-coated with gold at 40mA prior to observing under SEM. Morphologies of the scaffold were also characterized in hydrated condition using an inverted microscope (Nikon TE2000, Melville, NY) outfitted with a CCD camera. Digital micrographs were captured at different locations and were analyzed for pore area, pore size (major axis) and shape factor using Sigma Scan Pro 5 software. For each condition, more than 50 pores were analyzed. (**Figure 3.2**)

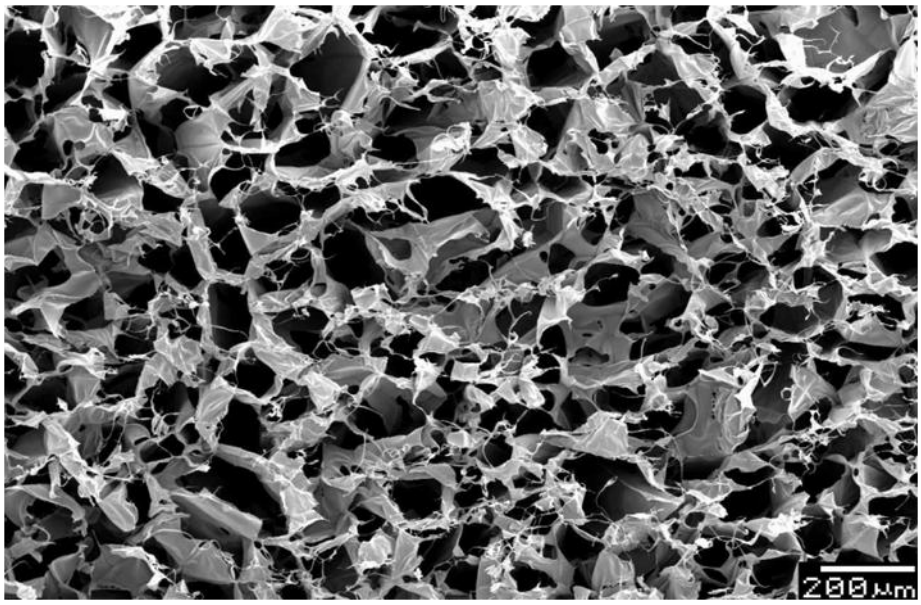

Figure 3.2: SEM images of Chitosan-Gelatin porous structure 0.5%-0.5%.

To determine the porosity of the scaffold, 10 mm × 50mm strips were cut and the thickness was measured using Vernier calipers. These strips were then weighed to get the dry weight. Next, the scaffold strips were neutralized with absolute ethanol to remove acetic acid. In order to remove all the air bubbles from scaffold strips, they were cyclically pressurized and depressurized manually while keeping them immersed in ethanol. These strips were weighed to find out their wet weight. Porosity of the structure was obtained by using formula:

$$\varepsilon p = \frac{W_{wet} - W_{dry}}{\rho_{et}} \times 100 \qquad (3.1)$$

where, W_{wet} is the weight of the ethanol wetted scaffold strips, W_{dry} is the weight of the dry chitosan-gelatin scaffold strips, ρ_{et} is the specific gravity of ethanol.

3.2.4 Alternative Designs:

Two new designs were investigated having 'split flow' arrangement (**Figure 3.3**). These designs had a parallel channel to scaffold from where the nutrients would flow;

a) *Design 7* had greater overall thickness of 4 mm, which allowed the nutrients to flow over a 2 mm open area (termed open channel) in addition to the 2 mm scaffold.

b) In *Design 8a,* a 2 mm cavity was introduced to place the scaffold by only increasing the reactor thickness at the location of the scaffold to 4mm, while leaving the inlet and outlet extensions to 2 mm. This modification was intended to protect the scaffold edges from the direct impact of the convective force while keeping the 2 mm open channel flow and 2 mm porous structure flow, similar to *Design 7*. Cavity like configuration and has 2 mm thick inlet and outlet channels.

Design 6 was also simulated to compare the results and had an increased number of mesh nodes compared to previous reports.

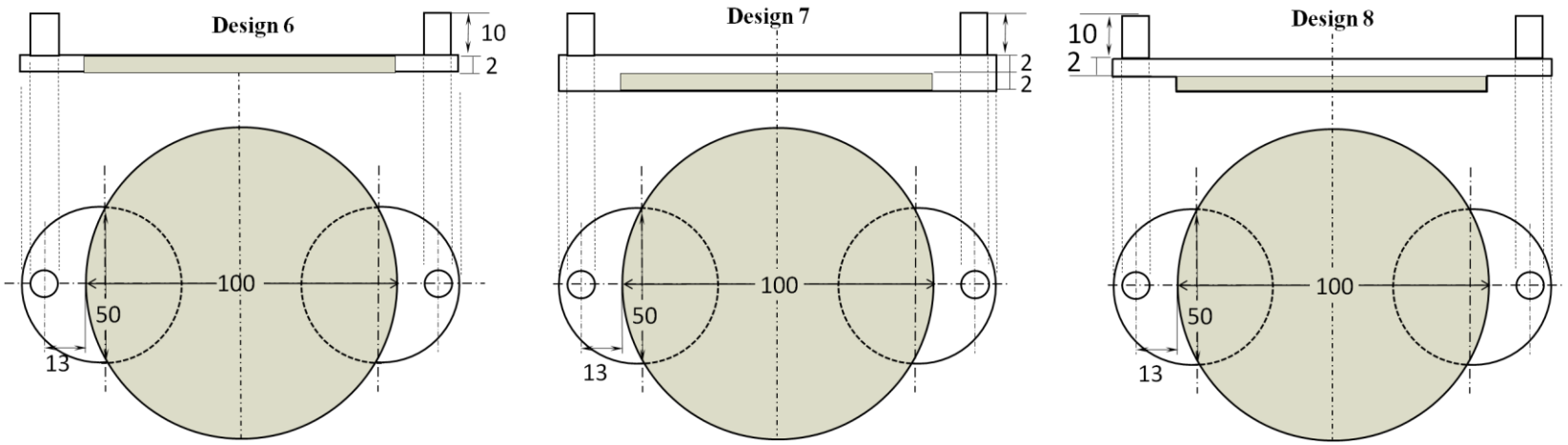

Figure 3.3: Schematic of alternate reactor designs. (The gray region signifies the location of scaffold)

3.2.5 Simulating fluid flow in the reactor:

The design geometries were created using COMSOL Multiphysics 3.5a (COMSOL, Inc., Burlington, MA). For this purpose, work plane settings option in the draw tab was used; which allows drawing of a 2D reactor model that can be extruded to create a 3D reactor model in the 3D model view. Next, the sub-domain and boundary conditions were set in the Physics tab. The steps similar as described in the manual given at the end of this manuscript were followed. To create a uniformly sized fine mesh for getting accurate results, the central reactor portion was divided into 8 layers of 0.5 mm each. The meshing of top most layer (boundary) was done using *Free mesh parameters* by selecting a *triangular mesh* type and by keeping maximum element size to 0.005m. Then *swept mesh parameter* was used to mesh the whole geometry. This technique gives increased number of nodes at which the Navier-Stokes equations are solved. Due to larger geometry of the new designs and the method of meshing, the number of Degrees of Freedom for Navier-Stokes equation and for convection and diffusion equations increased tremendously. Therefore the simulation became memory intensive. The computer which was used for simulation had a 1.86GHz Intel® Core™ 2 Duo processor with 32-bit Windows XP™ operating system. This did not allow the full utilization of available RAM. So, a 64-bit Windows Vista™ Ultimate operating system was used.

All simulations were performed under steady state conditions. The inlet conditions were set according to 1mL/min flow, while the walls were described as smooth with no slip condition. The outlet of the reactor was set at atmospheric pressure. The Reynolds number was calculated in the open channel region. It was found that the Reynolds number was in the range of 0.16 to 0.5. Hence, the flow through the open channels of the design was in laminar flow region.

Fluid flow through the porous structure was modeled using the Brinkman equation, which is given as

$$\mu\nabla^2 u_s - \frac{\mu}{\kappa}u_s = \nabla p \tag{3.2}$$

$$\nabla . u_s = 0 \tag{3.3}$$

where κ is the specific hydraulic permeability of the porous medium, u_s denotes the fluid superficial velocity vector, p is the fluid pressure, and μ the effective viscosity in the porous medium (Truskey et al. 2004). The hydraulic permeability (κ) is a geometric characteristic of the porous structure at several length scales (Truskey et al. 2004). The hydraulic permeability was calculated using 80μm and 140 pores/mm^2 and by using the equation

$$\kappa = \frac{\pi}{128} n_A d^4 \tag{3.4}$$

where n_A is the number of pores per unit area and d is the pore diameter assuming that the pores are circular in shape. The Navier-Stokes equations describing the flow in the open channel at steady state is given by

$$\rho(u.\nabla)u = -\nabla.\left[-\tau + p\delta_{ij}\right] \tag{3.5}$$

$$\nabla . u = 0 \tag{3.6}$$

where, ρ is the fluid's density (kg/m^3), p is the pressure (Pa) , δ_{ij} is the Kronecker delta function, τ is the shear stress and is given by shear stress tensor equation

$$\tau = \eta(\nabla u + (\nabla u)^T) \tag{3.7}$$

where η is the dynamic viscosity (Pa-s) and u is the velocity in the open channel (m/s). To account for the porous nature of the scaffold, the hydraulic permeability (κ) and void fraction (ε_p) were incorporated into equation (3.5) to give new form of Brinkman equation

$$\frac{\eta}{\kappa}u = -\nabla.\left[\frac{-\tau}{\varepsilon_p} + p\delta_{ij}\right] \tag{3.8}$$

3.2.6 Simulating nutrient consumption in the reactor:

Continuity equation in the chemical reaction engineering module of COMSOL 3.5a was solved to obtain the concentration profiles of oxygen and glucose by using results from steady state velocity profile of the nutrient flow in the reactor. Concentration of nutrients at different locations inside the porous region was obtained by solving the convective diffusion equation.

$$\nabla.(-D\nabla c_A) + u.\nabla c_A = r_A \tag{3.9}$$

where c_A is concentration of the nutrient (mol/m^3), r_A is rate of reaction of the nutrient (mol/m^3.s), D is the effective diffusivity of the nutrient (m^2/s), and u is the velocity vector (m/s). Nutrient medium was assumed to have properties of water, as water constitutes most of the bulk phase. The reaction term was only defined for the porous region of the reactor, i.e. only where the scaffold sits, as the cells would only be seeded on the scaffold.

Michaelis-Menten rate law kinetics was used to define the consumption of both oxygen and glucose. The rate law is given by the equation as follows,

$$-r_A = \frac{v_m C_A}{k_m + C_A} \tag{3.10}$$

where r_A is the reaction rate, v_m is the maximum reaction rate, and k_m is the Michaelis-Menten constant. In simulation, instead of c_A oxygen is denoted at c_1 while glucose is denoted as c_2.

The kinetic parameters of for glucose consumption were retrieved from Alpert et al (Alpert et al. 2002) based on the cells cultured on tissue cultured plastic, while the kinetic parameters for oxygen were calculated using the partial pressure vs time plot by Motterlini et al (Motterlini, Kerger et al. 1998). These kinetic parameters **(Table 3.1)** were calculated for cell density of 1.2×10^{12} cell/m^3.

Table 3.1: Kinetic Parameters for Smooth muscle cells (SMCs).

Cell Type	Oxygen		Glucose		Inlet concentrations	
	k_m(mol/m^3)	v_m(μmol/m^3.s)	k_m(mol/m^3)	v_m(μmol/m^3.s)	Oxygen (mol/m^3)	Glucose (mol/m^3)
SMCs	0.205	31.6	0.93	48.6	0.199	5.5

The concentration of oxygen and glucose at the inlet is given as:

$$c_i = c_{i0,inlet} \tag{3.11}$$

The initial concentration of oxygen in the growth medium was determined using the Henry's law constant at 37°C for each cell type. Initial concentrations of glucose were based on the growth media formulations used for populating SMCs. Mass transport at the outlet was assumed to be dominated by convection with negligible contribution from diffusion i.e.

$$n.c_i u = r_A \tag{3.12}$$

At all other boundaries, insulating conditions were specified as

$$\eta.(-D_i \nabla c_i u) = 0 \tag{3.13}$$

where D_i is the diffusivity and c_i is the concentration of particular nutrient i.

3.2.7 Physical properties and operating conditions for the reactor designs:

The nutrient medium used for providing nutrition to the cells has bulk amount of water. Hence, physical properties of the nutrient medium are assumed to be same as the physical properties of water at 37^0C. These values (**Table 3.2**) are used in the simulation.

Table 3.2: Physical properties and operating conditions

Property	Value
Density (rho)	1000 (kg/m^3)
Viscosity (eta)	0.006915 (N-s/m^2)
Pressure (Outlet)	1 atm
Temperature	37^0C

3.3 Results and Discussion

3.3.1 Effect of scaffold position inside reactor on pressure drop and shear stress:

The differential pressure and shear stress values for the *Design 6* (Devarapalli et al. 2009) showed 47.5 Pa and 983 µPa, respectively. When *Deign 7* was evaluated (**Figure 3.4**), it was seen that the pressure drop across the reactor reduced to 0.014 mPa, while in *Design 8a* the pressure drop was 0.0471 mPa. The shear stresses in *Design 7* was (**Figure 3.5**) at a uniform low value of 45.8 µPa, while in *Design 8a* the shear stress had a uniform higher value of 193 µPa in the region where scaffold sits. The increase in the shear stress in *Design 8a* can be attributed to the change in the thickness of the reactor. Compared to *Design 7*, *Design 8a* can provide a higher uniform stresses which is favorable for tissue growth and regeneration. Also the maximum shear stresses decreased from 442 µPa to 193 µPa in x-direction and from 983 µPa to 249 µPa in y-direction in *Design 8a* as compared to Design 6.

In *Design 6*, the maximum shear stress values in x-direction were 442 µPa and 0.055 µPa at 1.5 mm and 0.5 mm from the bottom of the reactor respectively and shear stress values in y-direction were 185.16 µPa and 185.2 µPa at 1.5 mm and 0.5 mm from the bottom of the reactor respectively. Also the maximum velocity in x-direction (along the flow) were 3.804×10^{-4}m/s, 4.589×10^{-4}m/s, 3.804×10^{-4}m/s at 1.5 mm, 1mm and 0.5 mm thickness from the bottom of the reactor respectively in *Design 6*. In *Design 6*, the flow of fluid is through the porous structure which explains the reason for the stress value to be near zero at the center of the porous structure. The difference in shear stresses between 1.5 mm and 0.5 mm can be attributed to the nature of velocity profile. As the flow is not completely developed the velocity at 1.5 mm from the bottom is higher as compared to the velocity at 0.5mm from the bottom and hence higher value of stress.

In *Design 7*, the shear stress values in x-direction were 240 µPa, 4.36 µPa, 3.86 µPa at 2mm, 1.5mm and 1mm thickness from the bottom respectively. The maximum shear stress values in y-direction were 139.5 µPa, 2.03 µPa, 1.0 µPa at 2mm, 1.5mm and 1mm thickness from the bottom respectively. While the maximum velocity in x-direction (along the flow) were 1.407×10^{-4}m/s, 1.302×10^{-4}m/s, 1.035×10^{-4}m/s at 2mm, 1.5mm and 1mm thickness from the bottom of the reactor respectively in *Design 7*.

In *Design 8a*, when the maximum shear stress values in x-direction were compared layer by layer it was observed that the values were 205 µPa, 0.014 µPa, 1.85×10^{-3} µPa at 2 mm, 1.5 mm and 1mm thickness from the bottom of reactor respectively. The maximum shear stress values in y-direction were 125 µPa, 0.9 µPa, 0.154 at 2 mm, 1.5 mm and 1mm thickness from the bottom respectively. In *Design 8a*, also the maximum velocity in x-direction (along the flow) is 1.726×10^{-6}m/s, 3.497×10^{-7}m/s, 1.119×10^{-7}m/s at 2 mm, 1.5 mm and 1 mm thickness

from the bottom respectively. These low velocities in *Design 8a* can be attributed to the *split channel* nature of flow. The shear stress values increase in the z-direction with top most layer being exposed to maximum stress. This is in accordance with the shear stress developed due to Newtonian fluids. **Figure 3.6** summarizes the results.

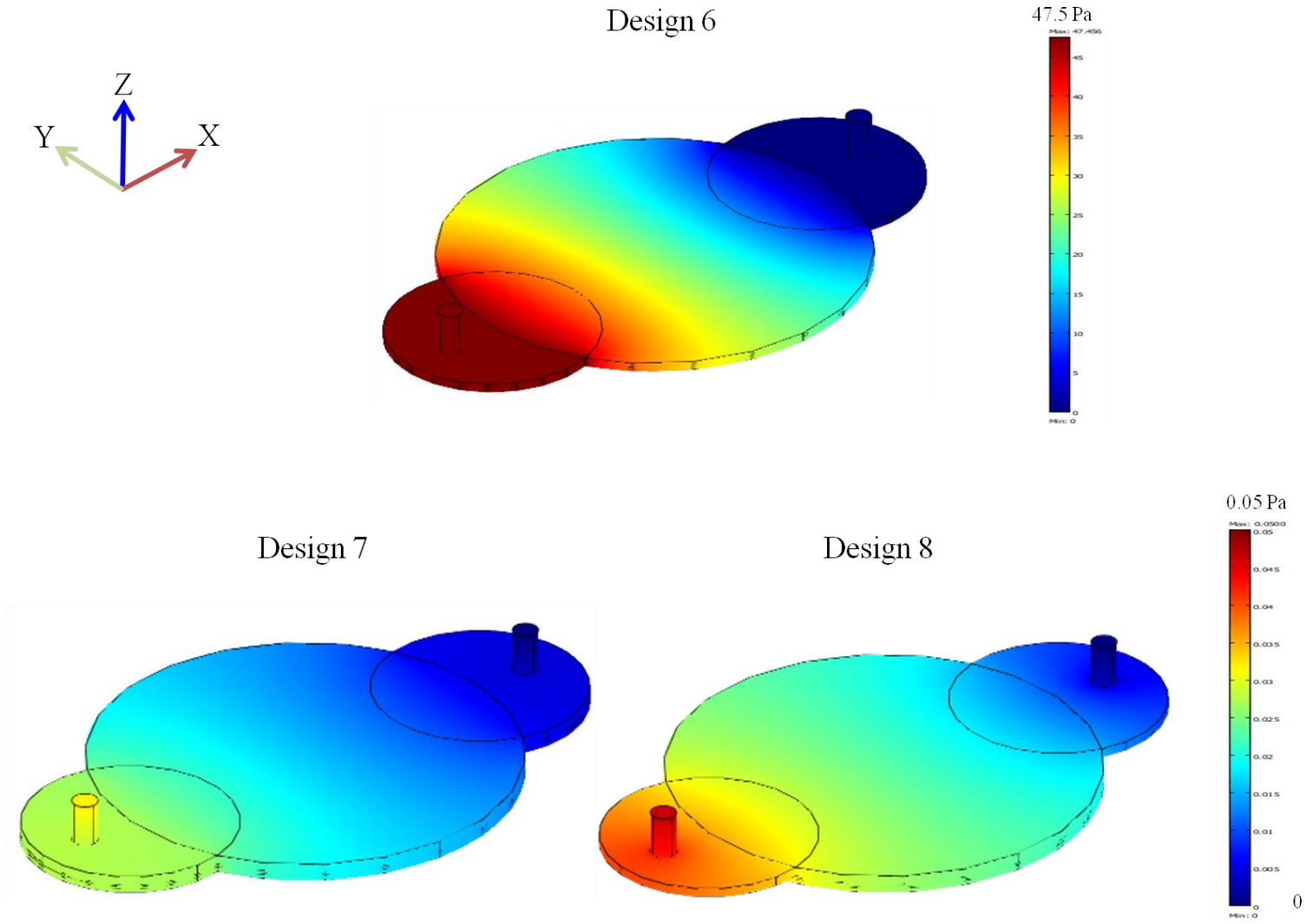

Figure 3.4: Comparison of pressure drop in Design 6, Design 7 and Design 8a at 1mL/min nutrient flow rate.

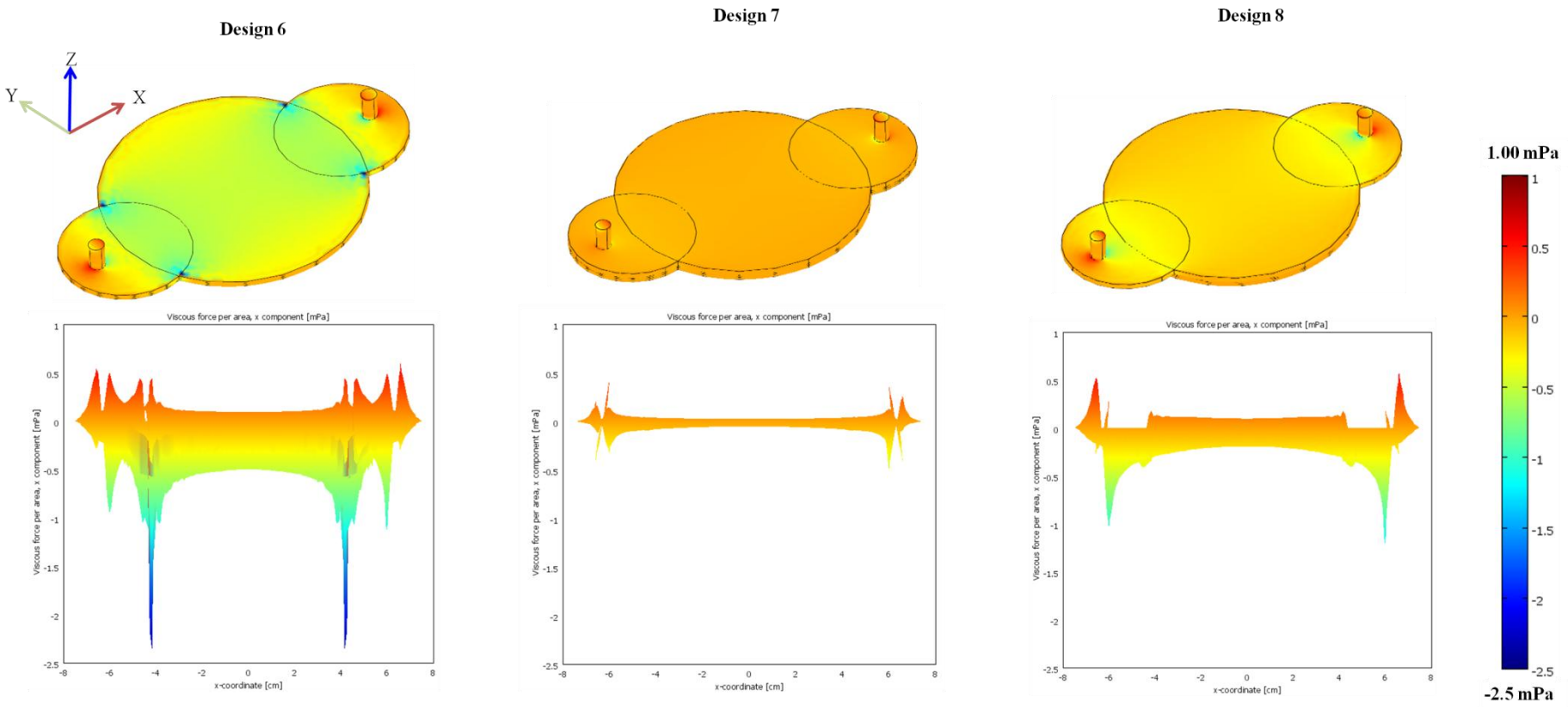

Figure 3.5: Comparison of shear stress distribution long x-axis in Design 6, Design 7 and Design 8a at nutrient flow rate of 1mL/min. a) Upper panel shows wall shear stress b) lower panel shows shear stress along x-axis.

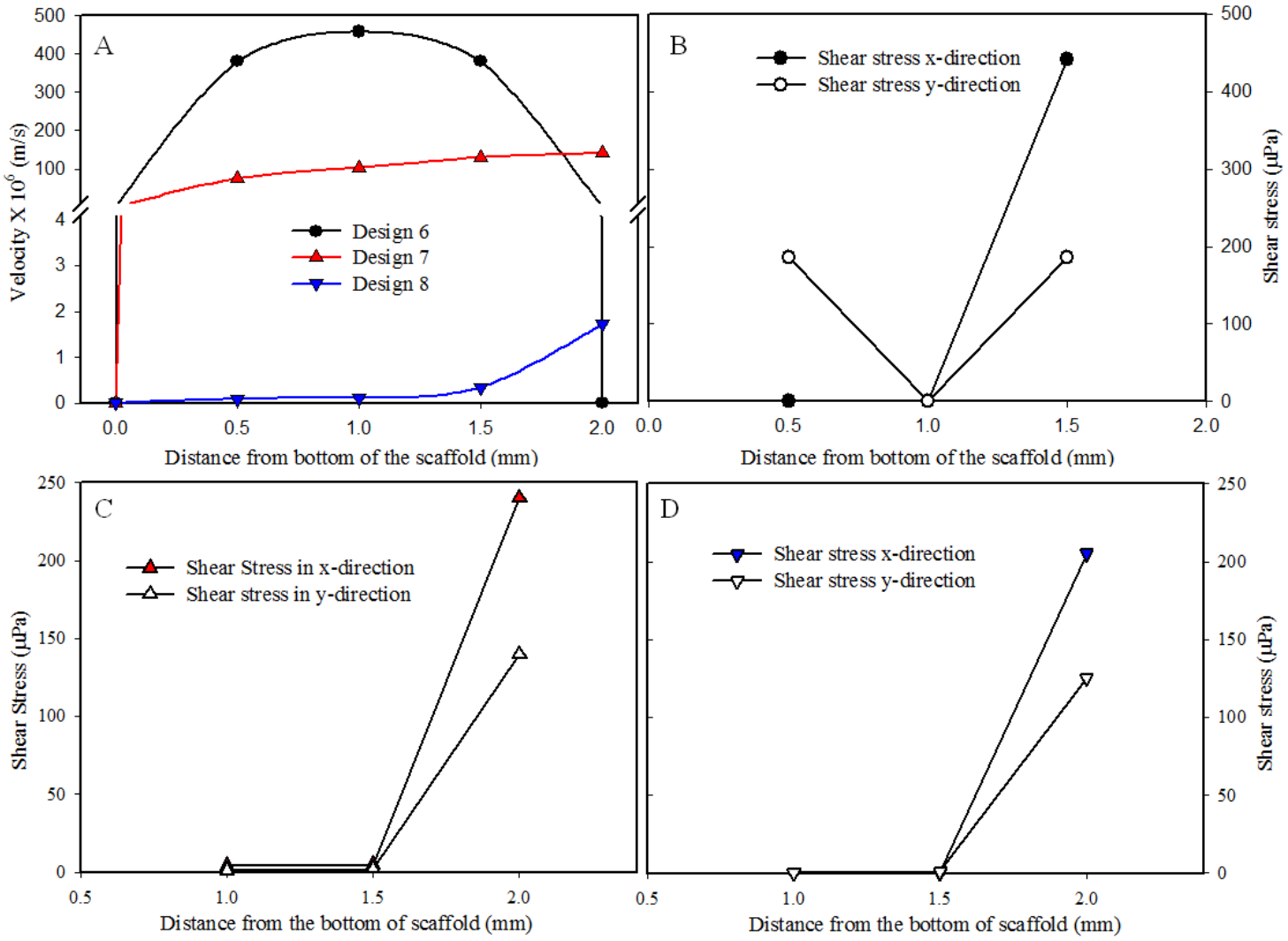

Figure 3.6: Comparison at various thicknesses in Design 6, Design 7 and Design 8a, at 1mL/min nutrient flow rate. A) maximum velocities in Design 6, 7 and 8. B) maximum shear stress in Design 6. C) maximum shear stress in Design 7. D) maximum shear stress in Design 8.

3.3.2 Effect of flow rate on pressure drop and shear stress:

The simulations for *Design 6* were performed at 1 mL/min flow rate and then increased gradually to 20 mL/min to assess the effects on the differential pressure. There was a non-linear increase in the pressure drop and shear stresses across the reactor in *Design 6* with increase in flow rate. However, in *Design 7* and *Design 8a* the values of differential pressure and shear stress increased linearly with the increase in the flow rate.

3.3.3 Effect of permeability on pressure drop and shear stresses:

During tissue healing, permeability of the porous structure will change due to the de novo deposition of the ECM, the proliferation of cells and degradation of the porous structure. To assess the effect of these changes in the scaffold, the pore size and porosity and hence the permeability values of the scaffold used in the simulations were decreased gradually. Comparisons were made at varying pore sizes up to 10μm for mimicking tissue regeneration at constant cell density. In Design 6, the pressure drop increased with reduced permeability and was inversely proportional to 1/k, as predicted by the Brinkman equation. However, there was no effect on the pressure drop across the reactor in Design 8a with reduced permeability. The shear stresses increased in a nonlinear manner as the pore sizes decreased in Design 6. However, the change was not as significant as the pressure drop.

3.3.4 Steady state concentration profile of the nutrients:

The rate law parameters for oxygen and glucose were used for analyzing nutrient consumption by smooth muscles cells. These simulations were performed at the same cell density (1.2×10^{12} cells/m^3). The comparison was also performed by reducing the porosity of the

scaffold from 85% to 10% and by keeping all other parameters same. Oxygen being the limiting reactant, the results were analyzed for oxygen distribution. Oxygen concentration profiles were plotted at incremental elevations of 0.5 mm from the bottom of the scaffold for each design. The concentration profiles of oxygen for *Design6* (**Figure 3.6**) showed uniform distribution of nutrients for porosity of 85% as well as for 10%. However, (**Figure 3.7**) the concentration of oxygen decreased remarkably throughout the scaffold in *Design 7* as the porosity reduced from 85 % to 10 %. In *Design 8a*, the concentration profiles of oxygen inside the scaffold remained the same for porosities of 85 %and 10 %.

These changes could be attributed to the altered convective characteristics in the new designs and the role of diffusion transfer in nutrient distribution. To understand these alterations, *Péclet* number was calculated using the equation:

$$Pe = \frac{L.V}{D} \tag{3.14}$$

where L is the characteristic length, V is the velocity while D is the effective diffusivity of the nutrient. Velocity was measured at the centre of the scaffold. These results (**Table 3.3**) showed that in *Design 7* the mass transfer inside the scaffold occurred both by convection as well as diffusion. When the porosity is 85 %, convective mass transfer is dominant but when the porosity is reduced to 10 % diffusive mass transfer becomes dominant. In *Design 8a*, the mass transfer inside the scaffold occurs primarily by diffusion as the scaffold is placed at a lower level and nutrients flow over it. As a result the concentration profiles do not change when the simulations are performed using constant effective diffusivities even if the porosity is reduced.

Table 3.3: *Péclet* number at the middle of the scaffold at 1mL/min flow rate.

	Porosity	**Distance from the bottom of the scaffold (mm)**			
		0.5	**1.0**	**1.5**	**2.0**
Design 6	For all	168.37	191.413	168.377	-
Design 7	85%	15.5607	53.6701	101.3089	148.3770
	10%	15×10^{-6}	25×10^{-6}	66×10^{-6}	34×10^{-5}
Design 8a	85%	0.02	0.06	0.25	1.57
	10%	15×10^{-6}	25×10^{-6}	66×10^{-6}	34×10^{-5}

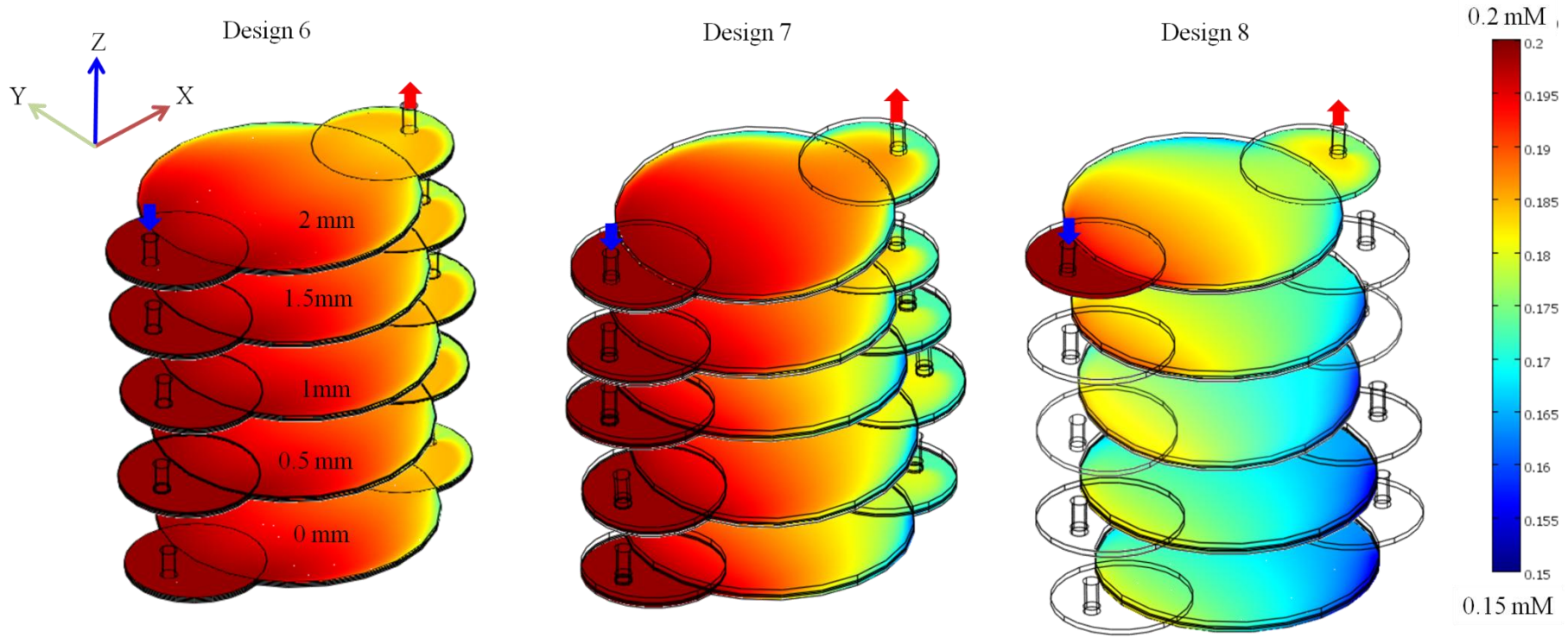

Figure 3.6: Oxygen concentration profile at porosity of 85 %for Design6, Design 7 and Design 8a at different thickness of the scaffold compared at 1mL/min of nutrient flow rate.

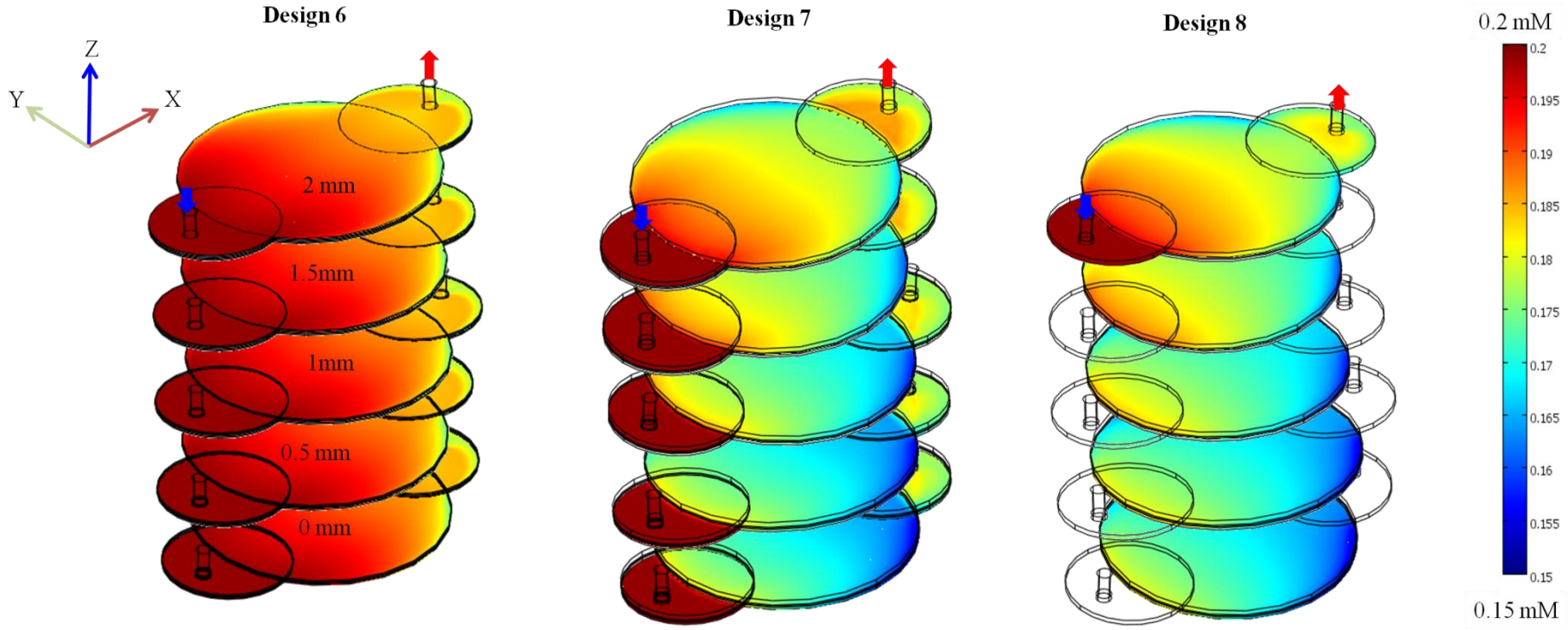

Figure 3.7: Oxygen concentration profile at porosity of 10%for Design6, Design 7 and Design 8a at different thickness of the scaffold compared at 1mL/min flow rate.

Since, as the earlier study (Devarapalli 2009) for *Design 6* was carried out using constant diffusivity values, it becomes necessary to take diffusivity changes into consideration, as the porosity of the scaffold would change due to the growing tissue. These changes need to be accommodated into the simulation for better estimation of nutrient distribution inside the porous scaffold.

CHAPTER IV

ASSESSING THE EFFECT OF DIFFUSIVITY CHANGES

4.1 Introduction:

In the previous chapter, the mass transport in *Design 8a* was determined to be diffusion limited. The diffusive process in a porous medium is affected by many factors, such as the molecular size of the nutrient, the presence of cells, the porosity and morphology of a scaffold (Zhou et al. 2010). During tissue regeneration process, several additional parameters will change the diffusive environment of the construct (Leddy et al. 2004). For example, the accumulation of newly synthesized extra cellular matrix reduces pore size of the scaffold, hindrance factor changes with pore size which will alter the effective diffusivity. Hence, molecular diffusion can become a constraint by limiting the nutrient supply required for cell proliferation and extracellular matrix production in a scaffold.

Earlier simulations were performed using constant infinite diffusivity values based on Stokes-Einstein equation. To account for diffusivity changes in the porous structure, diffusivity of glucose was measured experimentally using three different scaffolds of varying mass fractions. Further, effective diffusivity was evaluated using Mackie-Mearer relationship for a broad range of pore sizes and void fractions. Considering these changes in effective diffusivities,

simulations were performed using Design 8a in this study. In addition, three new bioreactor designs were investigated to accommodate varying thicknesses of scaffolds and permeabilities.

4.2 Experimental Analysis:

4.2.1 Preparation of porous scaffolds:

Three different concentrations of chitosan-gelatin solutions namely 0.5%-0.5% (wt/v), 1%-1% (wt/v), 2%-2% (wt/v) were prepared in 0.1M acetic acid using deionized water. Wells of 100 mm diameter were prepared on Teflon sheets using silicon glue, and 25mL of respective solutions were poured in the wells and frozen overnight at -80^0C. The frozen solutions were lyophilized overnight (Virtis, Gardiner, NY). The scaffolds formed from 0.5%-0.5% (wt/v) solutions has *skinny layer* on top which could be peeled off. For removing the skinny layer from scaffolds of 1%-1% (wt/v) and 2%-2% (wt/v) solution a wet paper was placed on the top of the solution, after pouring the solution inside the well, and was frozen along with the solution. After lyophilizing the paper was peeled off to generate scaffold without the skinny layer.

4.2.2 Characterization of pore size and pore number:

Obtained scaffolds were analyzed in dry condition using scanning electron microscope (SEM, Joel JSM 6360) at an accelerating voltage of 10 kV. For this purpose, small sections of dry scaffolds were sputter-coated with gold at 40mA prior to observing under SEM. Captured digital micrographs from random locations are shown in **Figure 4.1.** Morphologies of the scaffold were also characterized in hydrated condition using an inverted microscope (Nikon TE2000, Melville, NY) outfitted with a CCD camera. Digital micrographs were captured and analyzed for pore area, major axis, minor axis and shape factor (defined as $4\pi \times$ area/perimeter,

and when the number is closer to 1, the cell shape is closer to that of a circle) using Sigma Scan Pro 5 software. For each condition, more than 50 pores were analyzed.

The distributions of pore area, major axis, minor axis, and shape factor and were plotted as box plots to show the 10th, 25^{th}, 50^{th}, 75^{th}, and 90^{th} percentiles and the mean value (thick line within each box). Values that were outside 95^{th} and 5^{th} percentiles were treated as outliers. These results showed (**Figure 4.2**) that increased amount of chitosan and gelatin decreased the pore area, major axis, and minor axis. However, shape factor was not affected as the shape of the pores is regulated by ice crystals.

4.2.3. Estimation of Porosity:

To determine the void fraction of the scaffold, 10 mm × 50mm strips were cut from each scaffold and the thickness was measured using Vernier calipers. These strips were then weighed to get the dry weight and then washed with absolute ethanol to remove acetic acid. In order to remove all the air bubbles from scaffold strips, they were cyclically pressurized and depressurized manually while keeping them immersed in ethanol. These strips were weighed to find out their wet weight. Void fraction of the structure was obtained by using formula:

$$\varepsilon_p = \frac{W_{wet} - W_{dry}}{\rho_{et}} \times 100 \qquad (4.1)$$

where W_{wet} is the weight of the ethanol wetted scaffold strips, W_{dry} is the weight of the dry chitosan-gelatin scaffold strips, ρ_{et} is the specific gravity of ethanol. These results showed (**Table 4.1**) a reduction in the void fraction with increasing concentrations of polymers.

Table 4.1: Porosity of Chitosan-Gelatin scaffolds.

Scaffold	%Void fraction
0.5%-0.5% (wt/v)	92 ± 0.9
1%-1% (wt/v)	83±0.65
2%-2% (wt/v)	77±0.4

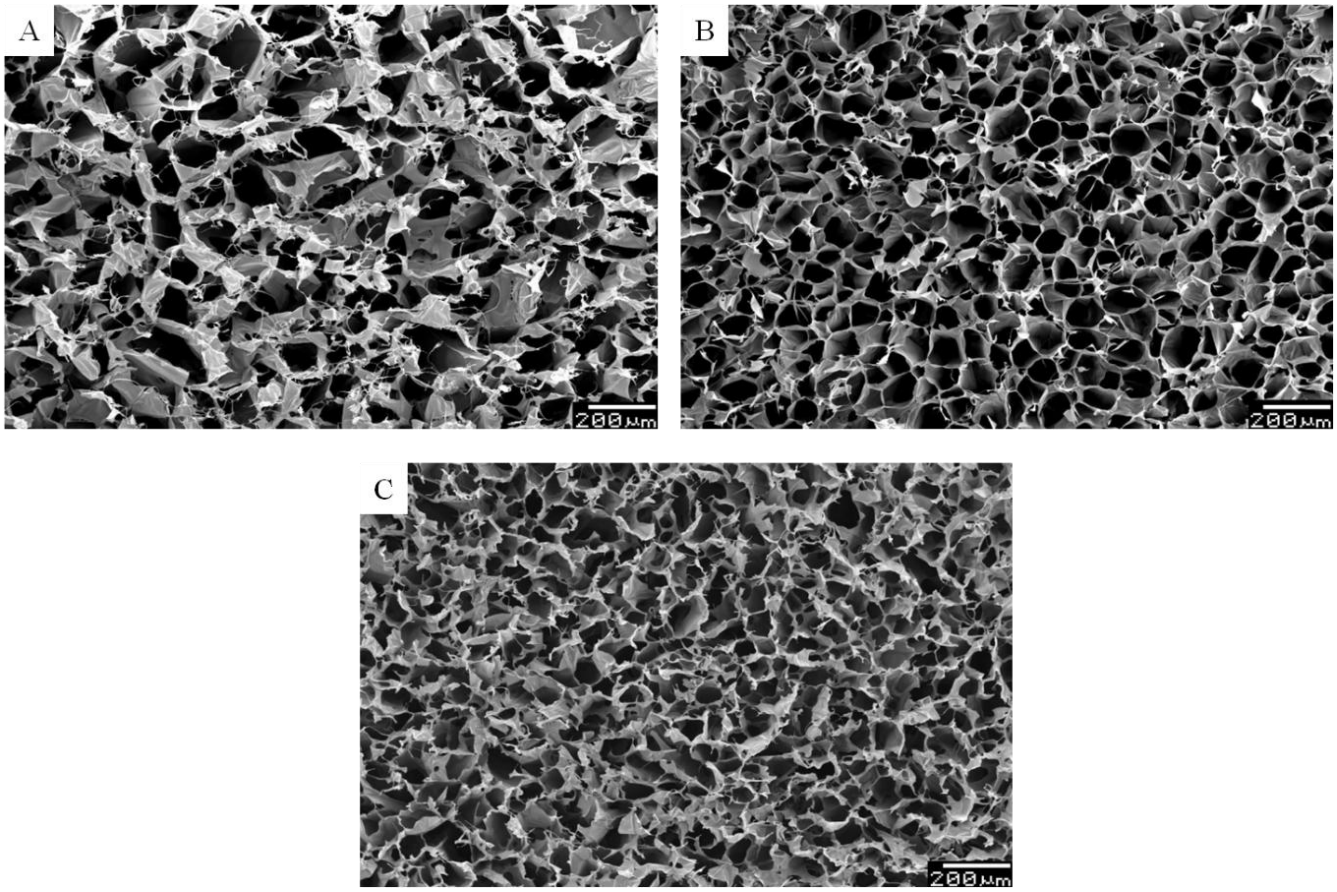

Figure 4.1: SEM images of chitosan-gelatin porous structure A) 0.5%-0.5% (wt/v) B) 1%-1% (wt/v) C) 2%-2% (wt/v)

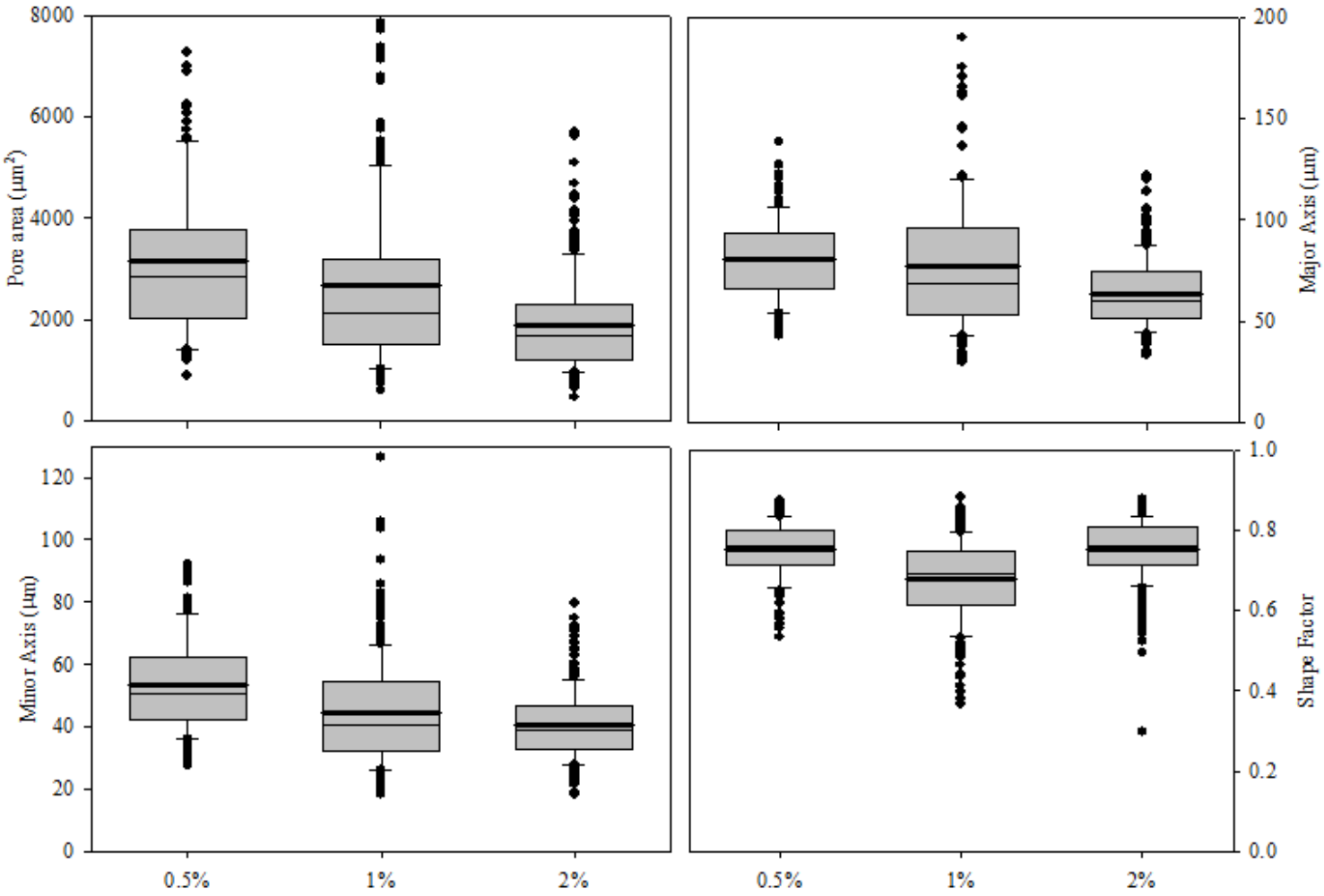

Figure 4.2: Box plot comparing pore area and pore size of 0.5%-0.5% (wt/v), 1%-1% (wt/v) and 2%-2% (wt/v) chitosan-gelatin scaffolds.

4.2.4. Permeability analysis of scaffolds:

Permeability analysis of chitosan-gelatin scaffolds was performed using glucose as the diffusing material, which is one of the nutrients. A diffusion cell apparatus (**Figure4.3**) was constructed in-house. The diffusion cell had two chambers, namely *Chamber 1* that contained glucose solution of known concentration (50 gm/L) prepared in deionized water, and *Chamber 2* contained DI water. Both the compartments contained exactly same volume of liquids (120 mL) during experiments and had a 3 mm diameter circular window for direct exposure of the scaffolds to the two solutions. These chambers were joined together using paper clips and the different chitosan-gelatin scaffolds were mounted in-between. The experiment was carried out at room temperature. The procedure during the entire experiment is as follows:

1) Hydrated Chitosan-Gelatin scaffold is mounted on one of the chambers. Second chamber is then clamped to the first chamber.

2) Known initial glucose concentration of 120 mL solution and 120 mL DI water were poured in Chamber 1 and Chamber 2, respectively. Both the chambers were kept well mixed using magnetic stirrers. Samples (100 µL) were taken from both the chambers after every 10 minutes for 1hour.

3) The collected samples were diluted to 1:9 ratio in DI water, for preparing them for the glucose analysis using *YSI-2700* Bio-scientific analyzer instrument.

4) The instrument setup consists of a glucose standard solution, a glucose buffer solution, a sampling chamber and a dipper tube. Glucose-oxidase membrane was used in *YSI-2700* Bio-scientific analyzer for determining glucose concentration. The instrument needed to be calibrated every time when turned 'ON'. After calibration, the instrument was setup

in automatic mode to pick one sample from the turntable and evaluate the glucose concentration.

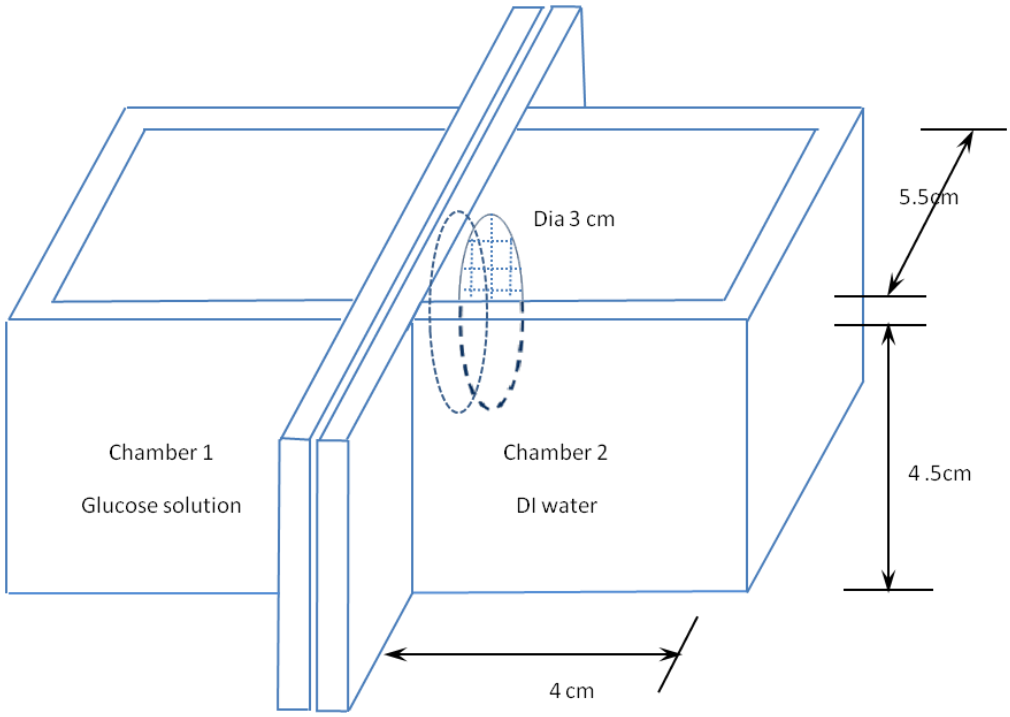

Figure 4.3: Schematic of diffusion cell

Using the glucose concentrations from various time points, membrane permeability was calculated as described previously (Raghavan et al. 2005). In brief, following equation was used assuming a quasi-steady state approximation

$$ln\left(\frac{C_0-2C_2}{C_0}\right) = -\left(\frac{A_m}{V}P\right)t \qquad (4.1)$$

where C_2 is the concentration of the glucose measured at any time t in Chamber 2, C_0 is the initial concentration in Chamber 1, A_m is the membrane area (= 9π/4 cm^2, as the radius of the chamber is 3 cm), V is the volume of each chamber (= 120 mL), and P is the Permeability of the

matrix. Then $\ln\left(\frac{C_0 - 2C_2}{C_0}\right)$ was plotted as a function of time from which the slope (= $A_m P / V$) was determined using a linear fit. The permeability (**Table 4.2**) was calculated using the slope values.

Table 4.2: Permeability's of various chitosan-gelatin scaffolds for glucose.

Scaffold	**Permeability 10^6 (m/s)**	**Diffusivity 10^9 (m^2/s)**	**Diffusivity 10^{10} (m^2/s) (Mackie-Mearer Approximation)**
0.5%-0.5%	7.9±0.04	13.6±0.04	69.3
1%-1%	2.0±0.06	7.2±0.06	48.0
2%-2%	1.2±0.05	4.7±0.05	37.4

However, it was noted that these experimental values of permeability and diffusivity for glucose through the chitosan-gelatin porous scaffold were an order of magnitude higher than the infinite diffusivity value calculated for glucose using Stokes-Einstein's equation. Hence, to estimate the diffusion coefficient of glucose through chitosan-gelatin scaffold, Mackie-Meares relation was used.

4.3. Computational Simulation:

4.3.1. Nutrient distribution in the reactor:

As described in the previous chapter, Design 7 and *Design 8a*geometrieswere created using COMSOL Multiphysics 3.5a (COMSOL, Inc., Burlington, MA). All simulations were performed under steady state conditions using similar boundary conditions and governing equations expect the diffusivity values.

The diffusivity of molecules through the porous structure is given by Mackie-Meares equation (Mackie and Meares 1955; Sengers et al. 2005).

$$D_{eff} = D_{\infty}\left(\frac{\emptyset}{2-\emptyset}\right)^2 \quad (4.2)$$

where, D_{eff} is the effective diffusivity, D_{∞} is the infinite diffusion coefficient of the solute from Stokes-Einstein equation and Φ is the porosity of the scaffold.

4.3.2. Importance of changes in diffusivity considerations on nutrient transport:

Using the effective diffusivity values for oxygen and glucose, simulations were performed. Comparison of oxygen distribution in *Design 8a* with and without diffusivity changes, showed significant differences (**Figure 4.4**) for a case of 50% void fraction. Simulations performed using free diffusivity showed no significant differences in oxygen concentration different elevations within the porous structure. However, simulations performed using effective diffusivity showed considerable changes in oxygen concentration at different elevations in the same reactor configuration. This confirmed the notion that *Design 8a* is diffusion limited.

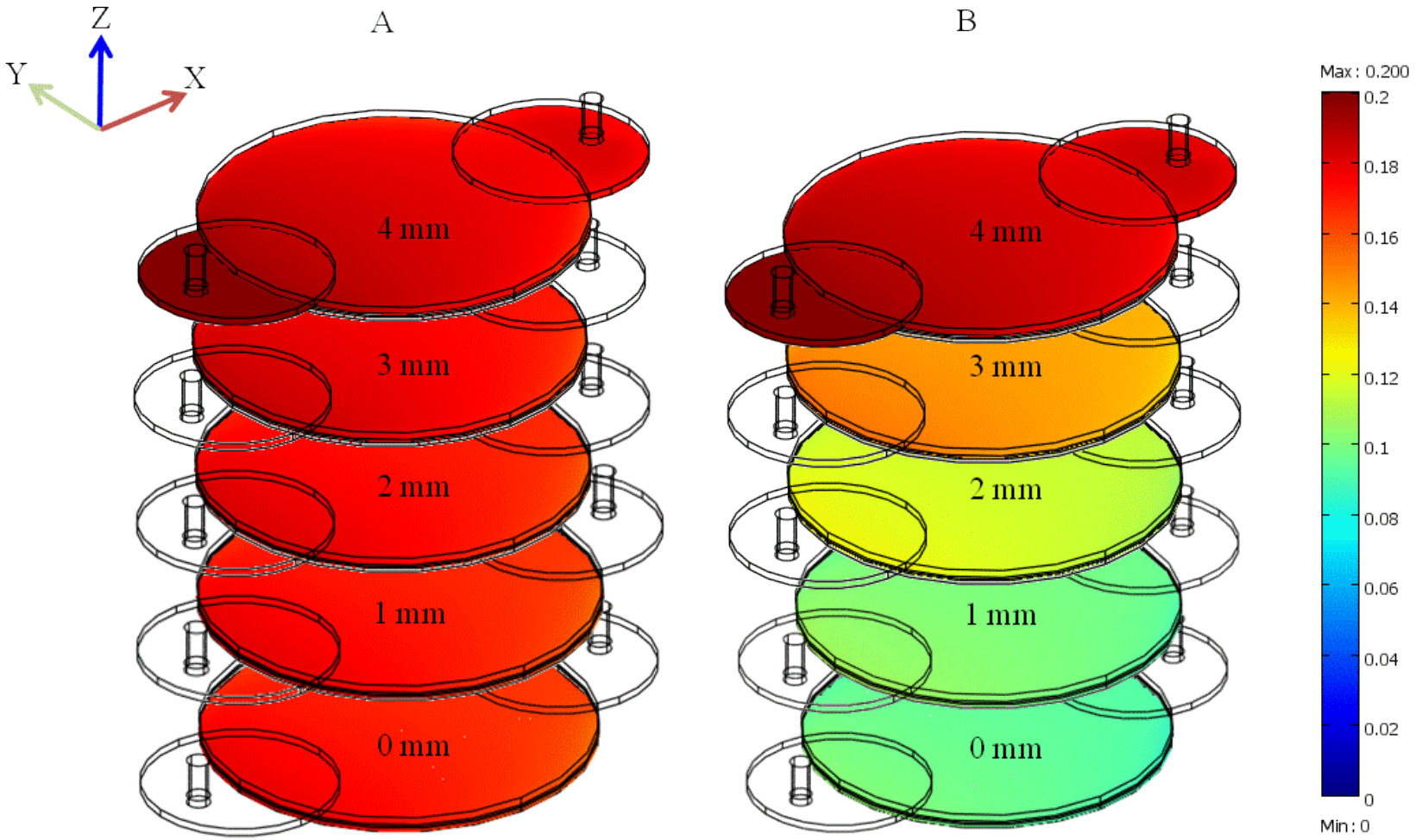

Figure 4.4: Comparison between concentration profiles of oxygen in *Design 8a* at 50 µm pore size and 50% porosity by using A) Free diffusivity B) Effective diffusivity calculated using Mackie-Meares relationship.

4.3.3 Understanding the effect of changing porosity on regenerating tissue:

To evaluate the effect of porosity changes during regeneration, simulations were performed in *Design 7* and *Design 8a* by progressively decreasing the pore size and porosity of the scaffold, i.e., in-turn decreasing the diffusivity of the nutrients according to the Mackie-Meares relation. The pressure drop and shear stress changes are expected to be similar to those observed in the previous chapter. Hence, they are not shown here. Significant changes in concentration of oxygen and glucose were observed at different elevations in the scaffold, similar to **Figure 4.5**. To better understand these changes, minimum concentrations were determined in each simulation and plotted for various permeabilities.

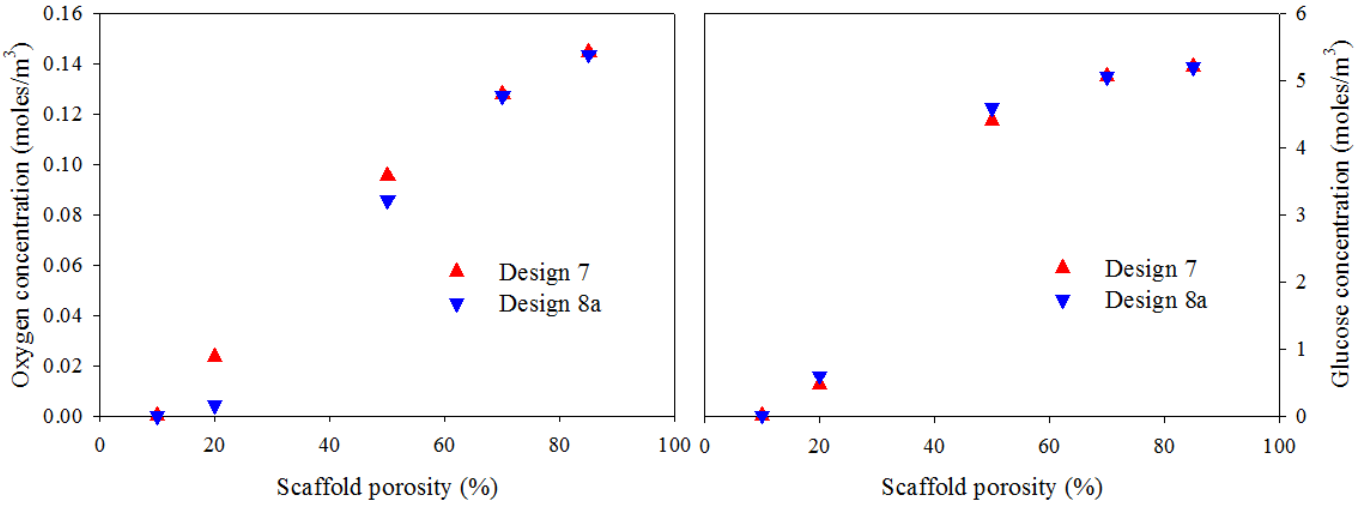

Figure 4.5: Effect of changing porosity on minimum O_2 concentration and glucose in *Design 7* and *Design 8a* at flow rate of 1mL/min and pore number of 140/mm^2. A) oxygen, B) glucose.

Both *Design7* and *Design 8a* showed comparable reduction in oxygen and glucose concentrations, with the reduced porosity. The minimum concentration of nutrients reduced drastically as the porosity of scaffold reduced further lower than 20 %. Since scaffold edges are

exposed to direct fluid flow in *Design*, the quality of the regenerated tissue could decrease. Hence, *Design 7* was not explored in subsequent analyses.

4.3.4 Understanding the effect of scaffold thickness:

Next, the effect of scaffold thickness was evaluated to understand at what thickness of the scaffold the concentration of oxygen approaches zero. *Design 8a* was modified to a 4 mm thick scaffold (*Design 8b*), and 6 mm thick scaffold (data not discussed) with all other configurations unchanged (**Figure 4.6**). These simulations showed that, the minimum oxygen concentration approached near zero value in *Design 8b* when the porosity was reduced to 50%. The difference in oxygen concentration profiles at various elevations for *Design 8b* at 85% porosity and 50 % porosity are shown in **Figure 4.7**. Also to check the effect of healing tissue, the pore size and porosity were decreased progressively. These results showed that the bioreactor configuration with only one channel is insufficient to provide nutrients during tissue regeneration. Hence, alternative configurations had to be explored.

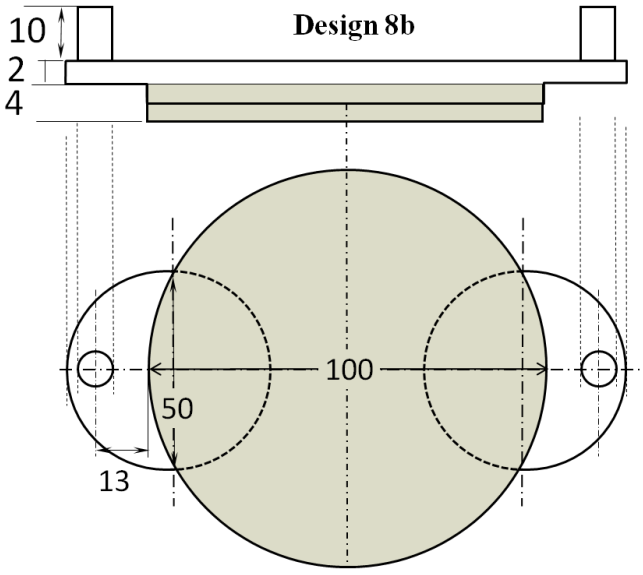

Figure 4.6: Schematic of *Design 8b* (gray region signifies the location of scaffold)

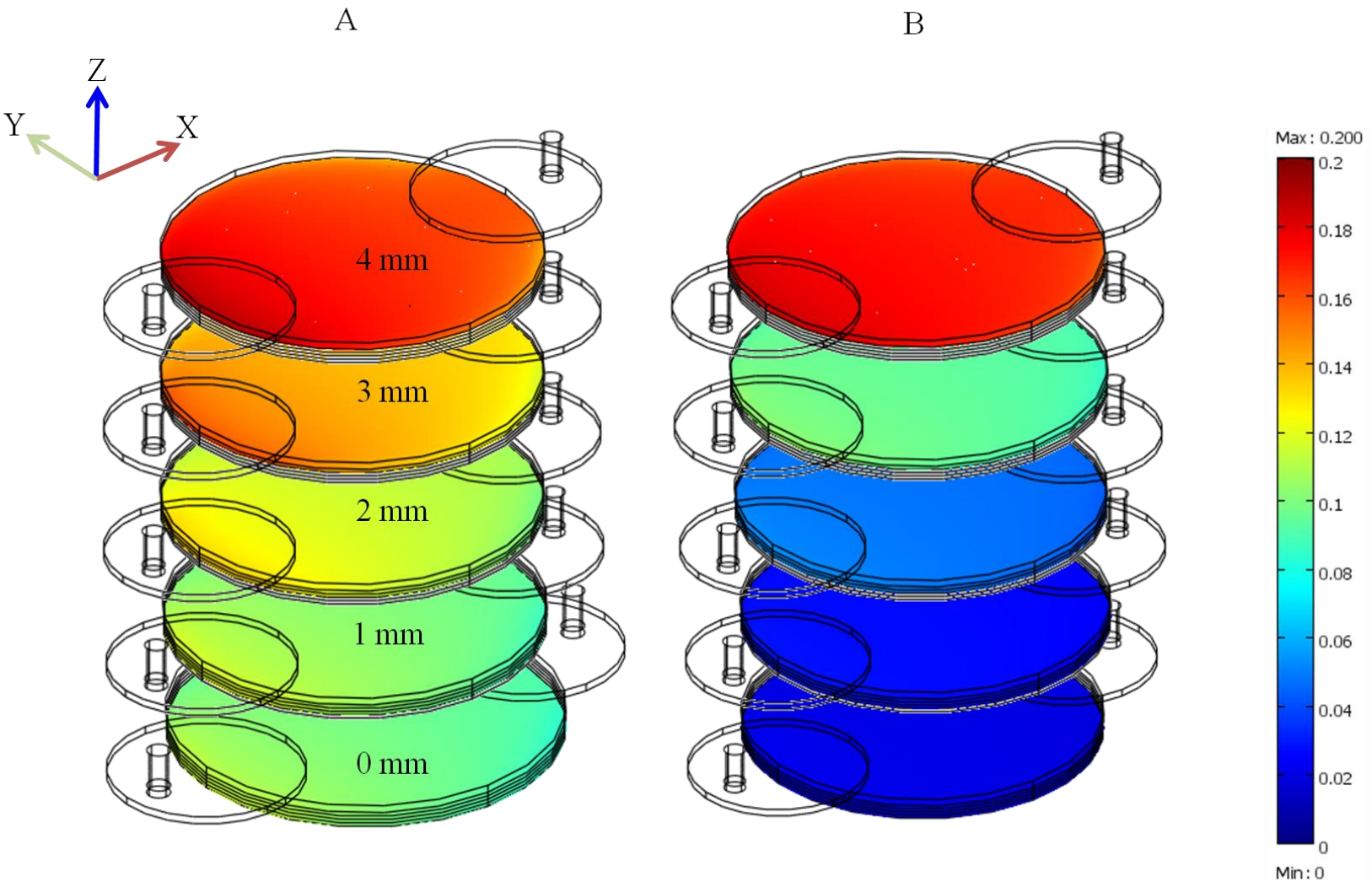

Figure 4.7: Oxygen concentration profiles in *Design 8* for 4 mm thick scaffold compared at 1mL/min flow rate for A) 85% porosity B) 50% porosity

4.3.5Assessing the effects of channel location:

Design 8 was modified to understand the effects of having the flow of nutrients from both sides of the scaffold, which would reduce the distance through which nutrients have to diffuse by half. This change in design corresponded to two parallel channels with scaffold sandwiched in between. Two modifications (*Design 9* and *Design 10)* were evaluated,

In *Design 9* (**Figure 4.8**), two separate inlets and outlets were incorporated with two 2 mm thickness channels on opposite sides. Three different thicknesses namely 2 mm (*Design 9a*), 4 mm (*Design 9b*) and 6 mm thicknesses were also evaluated

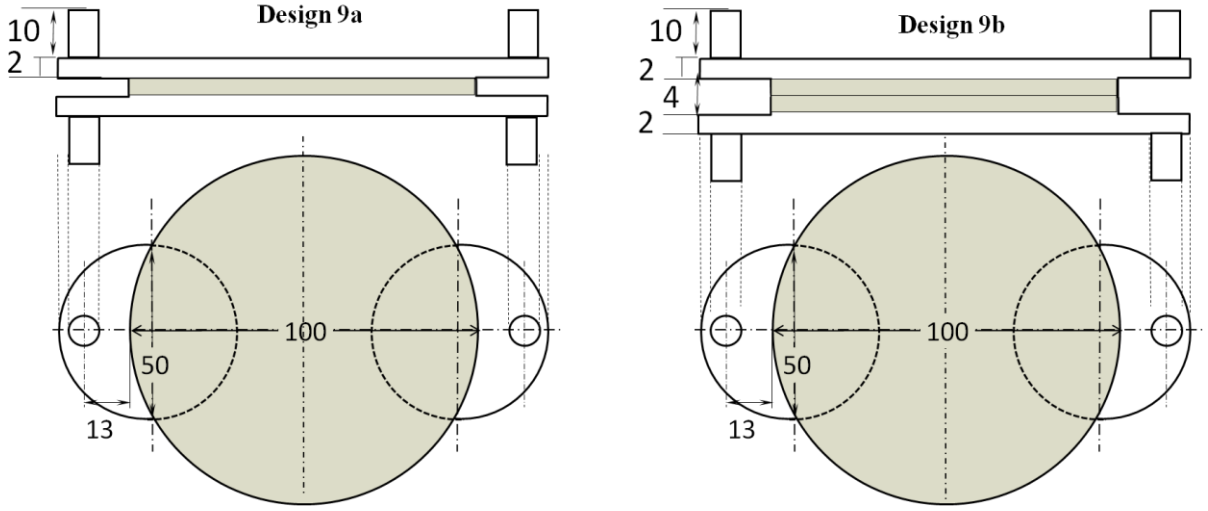

Figure 4.8: Schematic of Design 9 (gray region signifies the location of scaffold)

For practical purposes, placing the reactor horizontal may be important. For this purpose (**Figure 4.9**), another design (*Design 10*) with one inlet and one outlet but branching into two stream for the two channels of 2 mm thickness was considered. Similar to Design 9, three scaffold thicknesses namely 2 mm (*Design 10a*), 4 mm (*Design 10b*) and 6 mm thicknesses were evaluated.

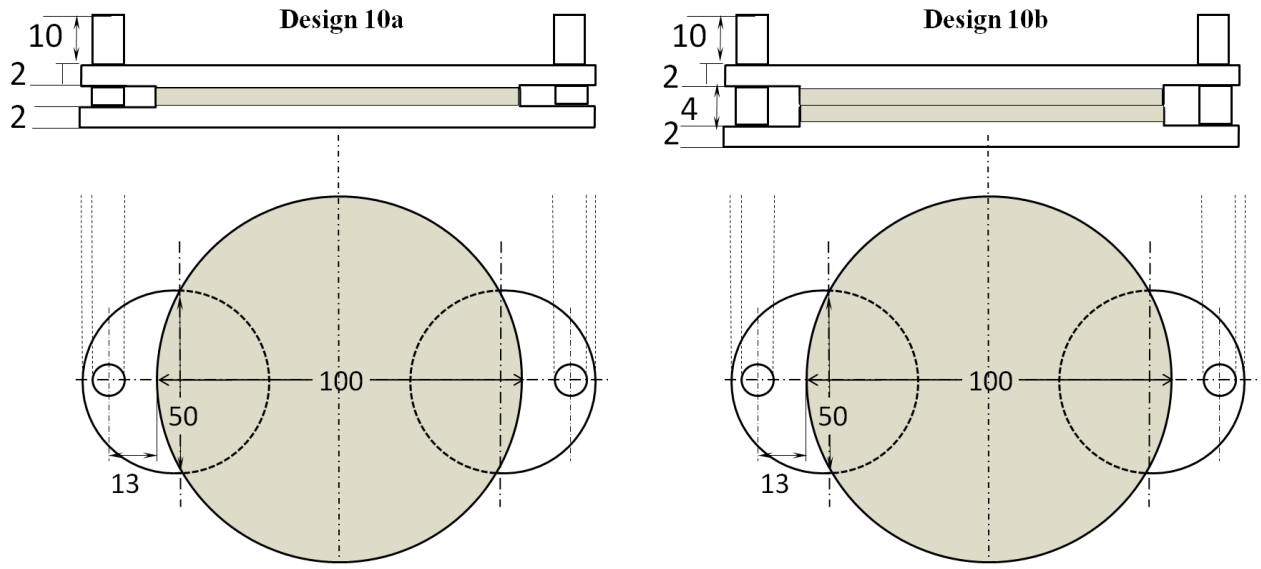

Figure 4.9: Schematic of Design 10 (gray region signifies the location of scaffold)

At 1 mL/min flow rate and varying porosity values, the simulations showed comparable minimum oxygen concentration and minimum glucose concentration (**Figure 4.10**) values for Design 9a and Design 10a. Design 9a had pressure drop and maximum shear stress values of 24 mPa and 112.5 µPa, respectively whereas *Design 10a* had pressure drop and maximum shear stress values of 28 mPa and 105 µPa. It can be seen that the there is not much difference in the results. Hence, only *Design 10* was considered for further analyses.

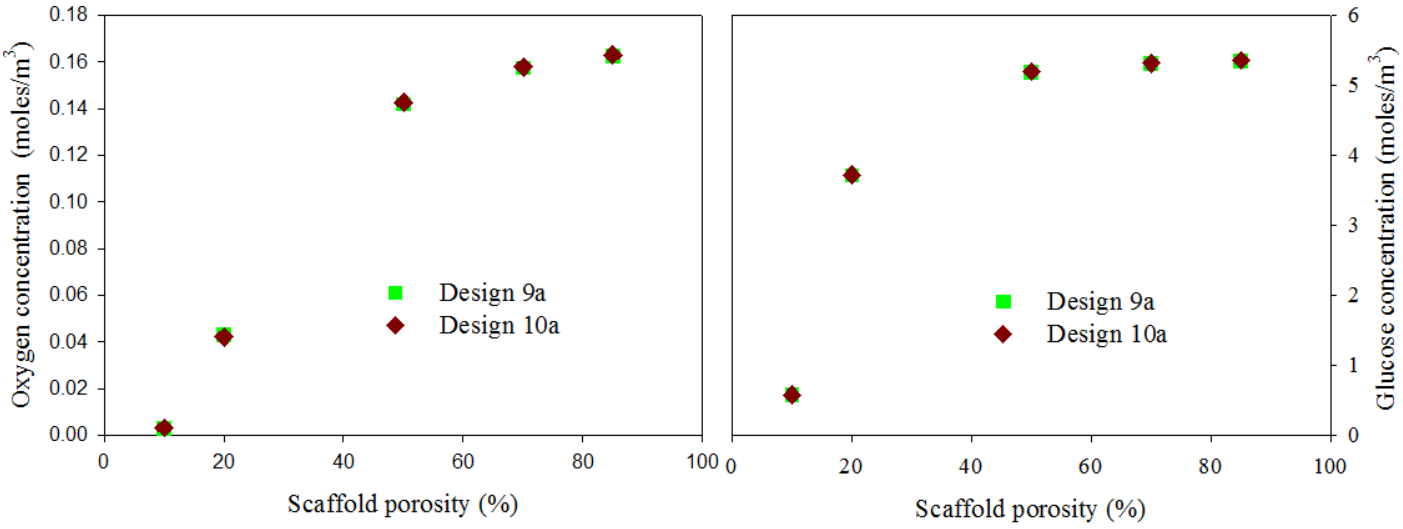

Figure 4.10: Effect of changing porosity on minimum nutrient concentration with 140pores/mm^2 and at flow rate of 1mL/min A) oxygen, B) glucose.

When scaffold thickness was increased to 4 mm (*Design 10b*), uniform nutrient distributions (**Figure 4.11**) were observed at various locations with 1 mL/min flow rate.

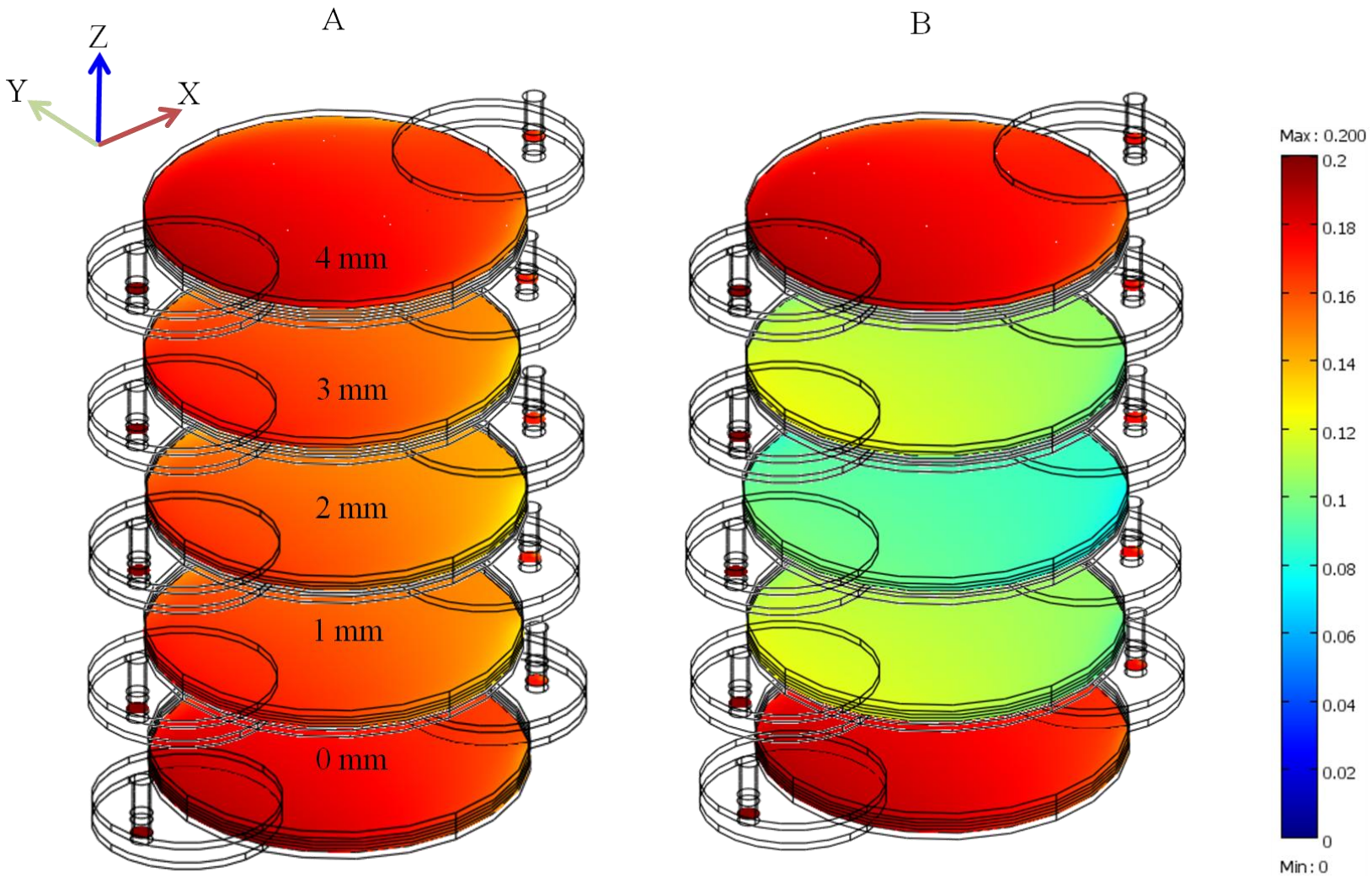

Figure 4.11: Oxygen concentration profiles in Design 10b (4 mm thick scaffold) compared at 1mL/min flow rate for A) 85% porosity B) 50% porosity

4.3.6Assessing the effects of channel height:

Adding 2 mm channels on both sides necessitates significant increase in the hold-up volume of expensive growth medium. One way to reduce the hold-up volume is to decrease the channel height. To test the effect of the changing the channel height, the new design (*Design 11)* had 1 mm thickness on both sides (**Figure 4.12**). This would reduce the hold-up volume of the nutrient media to that in *Design 8*, without compromising on the effectiveness of the reactor design. As before, two scaffold thicknesses namely 2 mm (*Design 11a*) and 4 mm (*Design 11b*) were evaluated.

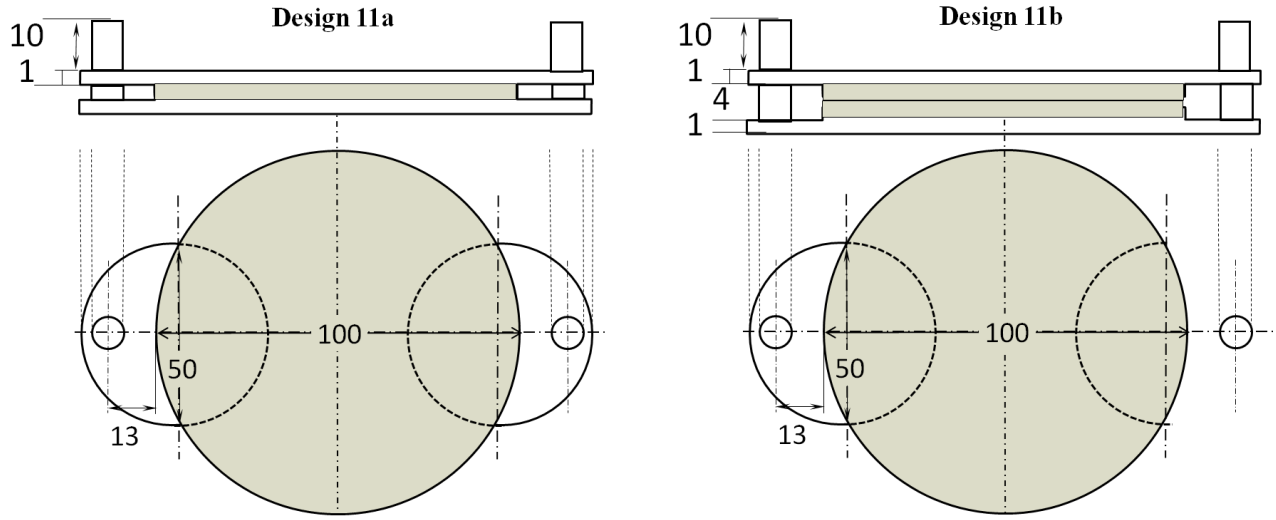

Figure 4.12 Schematic of Design 11 (gray region signifies the scaffold location)

These results showed no significant changes in nutrient concentrations for Design 11a and Design 10a. However, the pressure drop value increased to 156 mPa in case of *Design 11* from 24 mPa in case of *Design 10*. Even the shear stress values along x-direction increased to 446 µPa for Design 11 from 112 µPa for Design 10. Further, the simulation were run for 4mm scaffold i.e. for *Design 11b* and the minimum oxygen concentration results were compared to the

results of *Design 8b* in **Figure 4.13** and tabulated in **Table 4.3**. It was observed that *Design11b* had slightly higher pressure drop and shear stress values, while having better nutrient concentration profiles and higher 'minimum oxygen concentration' inside the scaffold than *Design 8b*.

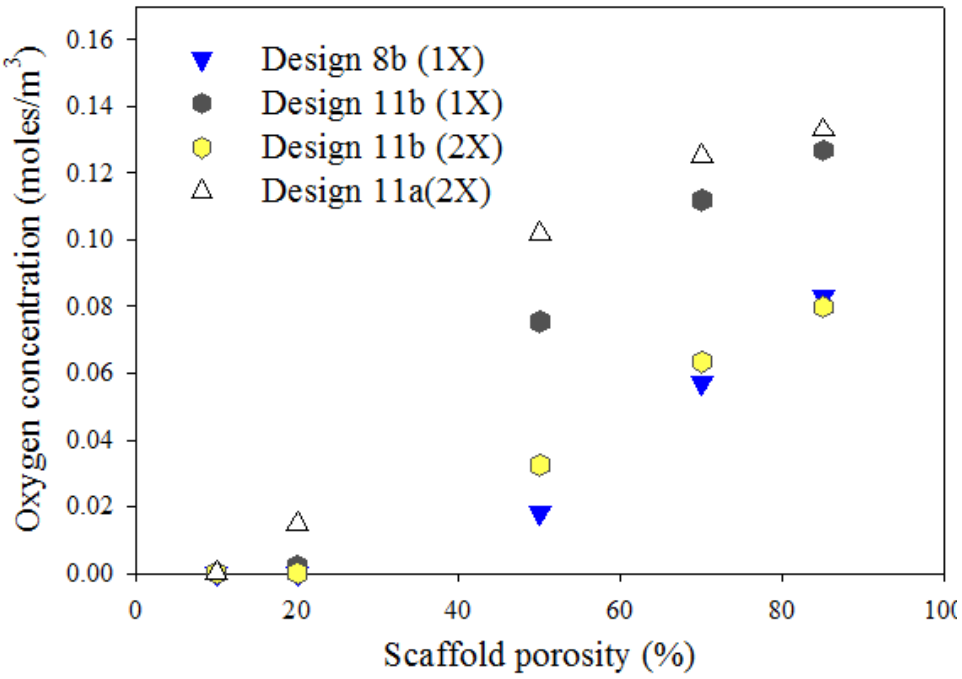

Figure 4.13: Effect of changing porosity on minimum oxygen concentration in Design 8b and Design 11b with 140pores/mm^2 and at flow rate of 1mL/min.

Table 4.3: Comparison between Design 8b and Design 11b (4 mm scaffold) at various pore sizes and porosity and at 140pores/mm^{2}pore number, (1.2×10^{12} cells/m^3) and 1mL/min flow rate.

Pore size (μm)	Porosity (%)	Hydraulic Permeability 10^{10}(m^2)	Oxygen Diffusivity 10^{10} (m^2/s)	Design 8b				Design11b			
				Minimum Oxygen concentration (μM)	Shear stress (μPa)		Pressure drop (Pa)	Minimum Oxygen concentration (μM)	Shear stress (μPa)		Pressure drop (Pa)
					Along x-axis	Along y-axis			Along x-axis	Along y-axis	
80	85	1.407	11.94	83	203.1	119.5	0.0489	127	389.5	233.5	0.156
80	70	1.407	6.33	55	203.1	119.5	0.0489	112	389.5	233.5	0.156
50	50	0.2147	2.43	18	203.5	119.4	0.0489	74	391.1	235.3	0.156
20	20	0.005497	0.27	0.004	203.5	119.4	0.0489	3.34	391.6	237.9	0.156
10	10	0.000343	0.06	0	203.5	119.4	0.0489	0	373.37	220.83	0.156

4.5.7 Assessing the effects of cell density:

Regeneration of tissue will cause the initial number of cells to increase, as the cells multiply. To access the effect of this increase in cell density on nutrient consumption, pressure drop and shear stress, simulations were performed on Design 11 by increasing the initial cell density of SMCs. The flow rate was kept constant at 1mL/min. Simulations were run for 2mm as well as 4mm scaffold thickness. These results (**Table 4.4**) showed that the minimum oxygen concentration reduced drastically with decreasing permeability at constant cell density. Insufficiency of oxygen concentration is reached at 10 μm pore size and 10 % porosity for a 2 mm scaffold. Whereas for a 4 mm scaffold, minimum oxygen concentration drops to zero at 20 μm pore size and 20 % porosity value. In addition, it was seen that the pressure drop across the reactor as well as the shear stress values did not change due to the change in cell density.

Table 4.4: Comparison between Design 11a (2mm scaffold) and Design 11b (4 mm scaffold) at various pore sizes and porosity and at constant cell number, 140pores/mm^{2}pore number and 1 mL/min flow rate.

Pore size (μm)	Porosity (%)	Hydraulic Permeability 10^{10}(m^2)	Oxygen Diffusivity 10^{10} (m^2/s)	**Design 11a (2 mm scaffold, 2.4×10^{12}cells/m^3)**				**Design11b (4 mm scaffold, 1.2×10^{12} cells/m^3)**			
				Minimum Oxygen concentration (μM)	Shear stress (μPa)		Pressure drop (Pa)	Minimum Oxygen concentration (μM)	Shear stress (μPa)		Pressure drop (Pa)
					Along x-axis	Along y-axis			Along x-axis	Along y-axis	
80	85	1.407	11.94	133	203.1	119.5	0.0489	79.8	389.5	233.5	0.156
80	70	1.407	6.33	125	203.1	119.5	0.0489	63.5	389.5	233.5	0.156
50	50	0.2147	2.43	102	203.5	119.4	0.0489	32.4	391.1	235.3	0.156
20	20	0.005497	0.27	15	203.5	119.4	0.0489	0	391.6	237.9	0.156
10	10	0.000343	0.06	0	203.5	119.4	0.0489	0	373.37	220.83	0.156

4.4 Discussion:

In this study, changes in diffusivity due to the process of To account for changes in diffusivity values due to changes in porosity of the scaffold, glucose diffusivity experiments were carried out using scaffold of three different compositions and hence three different porosity values. Since these values of diffusivities were determined to be a magnitude higher than, effective diffusivity, the diffusion coefficient of nutrients through the porous scaffold was calculated using Mackie-Meares equation. These effective diffusivity values were then incorporated into the simulations and the results compared. The results showed a fall in concentration profiles of nutrients for same reactor configuration when compared by keeping other parameters constant.

Further, the effectiveness of *Design 8* was tested for a 4 mm scaffold (*Design 8b*) and minimum concentration of oxygen was checked as oxygen is the limiting reactant. It showed that the minimum concentration of oxygen approached zero when the porosity of scaffold was decreased to 50 %, meaning this configuration of reactor would not support a 4mm thick growing tissue. So, in order to provide sufficient nutrients to the growing tissue of 4mm thickness, two new reactor configurations were explored. This first modification was named as *Design 9* which was provided with two channels having 2 mm thickness each and which had two separate inlets and outlets for both the channels. This design gave better results for the minimum oxygen concentration even for the 4mm reactor (*Design 9b*) when the porosity values were lowered as compared to *Design 8b*. However, the *Design 9b* was not considered for further analysis because of practical reasons of handling and mounting. *Design 10* with single inlet and outlet split into two streams which provided the flow to both parallel channels was studied and it was found

that the results obtained for *Design 9a* and *Design 9b* were similar to *Design 10a* and *Design 10b*.

For being consistent with the amount of nutrient media 'Hold-up' volume inside reactor, a new configuration, *Design 11*, was developed which had two channels each of thickness 1 mm. The simulation results of this design were at par with *Design 10* and were far better than Design8. Also, it was seen that the pressure drop across *Design 11* increased a little to 0.156 mPa and the shear stresses along the reactor also had a higher value than values for *Design 8*. Thee slightly increased shear stress value could be beneficial for the cell as seen by the researchers cited in this study.

CHAPTER V

CONCLUSIONS AND RECOMMENDATIONS

5.1 CONCLUSIONS

This study used a circular shaped parallel plate split flow reactor and evaluated different design for regenerating high aspect ratio tissue of 100 mm diameter and varying in thickness from 2 mm to 4 mm. The bioreactor system studied can be used for developing clinical grade skin and bladder tissues. Conclusions from the study are summarized as below according to the two specific aims.

Specific Aim 1*: *To determine alternate design for a flow through bioreactor.

1. To understand flow characteristics in flow through reactor configuration, simulations of *Design 6* and two new designs (*Design 7* and *Design 8*) of the circular shaped reactor were performed using COMSOL Multiphysics 3.5a (COMSOL, Inc., Burlington, MA). *Design 7* had greater overall thickness than *Design 6*, whereas *Design 8* had a scaffold placed inside a cavity like arrangement. Analysis of *Design7* and *Design 8*, suggested that, both the designs had a far lesser pressure drop as compared to *Design 6*.
2. When *Design 7* and *Design 8* were compared, *Design 7* has a slightly higher pressure drop value than *Design 8*.

3. The comparison of shear stresses along the reactors showed that, *Design 6* gave the highest shear stress value as compared to *Design 7* and *Design 8*. The shear stress values of *Design 7* and *Design 8* were similar. The spikes in sheer stress plot of *Design 8* can be attributed to the change in the cross section area in that region. Also, when the pore size and porosity was reduced to mimic the cell growth and extracellular matrix formation, the pressure drop and shear stress values for both *Design 7* and *Design 8* did not change.
4. After calculating *Peclet* number, it was found that through the scaffold in *Design 6* was convection dominant. Nutrient transport through scaffold in *Design 7* occurred due to convection as well as diffusion, when the porosity of the scaffold was high. However, when the porosity of the scaffold was lowered, the flow through scaffold becomes diffusion dominant. While, for *Design 8* the flow through the scaffold is always diffusion dominant. As diffusive mass transfer plays an important role in nutrient distribution, it was necessary to account for the changes in diffusivity values that would occur due to tissue regeneration.

***Specific Aim 2*: To assess the effect of diffusivity changes on nutrient transport.**

Permeability experiments were carried out in a diffusion cell apparatus which was built in-house. The values of the diffusion coefficient for glucose from these experiments were an order of magnitude higher than the infinite diffusion coefficient of glucose. So, the effective diffusion coefficients of nutrients were calculated using Mackie-Meares relation which estimates the diffusion of solutes through porous media.

1) Simulations for *Design 8* using infinite diffusivity values and diffusivity values from Mackie-Meares relation showed differences in concentrations profiles of nutrients. It can be said that the simulations using Mackie-Meares approximation for diffusivity predict the nutrient distribution in a better way.
2) Further it was seen that for a 4mm scaffold in *Design 8*, the minimum concentration of oxygen reduced drastically for lower values of pore size and porosity. So, two new designs *Design 9* and *Design 10*, with two parallel channels were considered. The two channels system in these designs reduced the length through which nutrients have to. Though, *Design 9* and *Design 10* gave similar results, *Design 9* was not considered further because of practical reasons of handling and mounting complications.
3) For a comparison with *Design 8*, *Design 11* was considered to keep the reactor 'Hold-up' volume same as with *Design 8*, without compromising on the effectiveness of the design. This modification, *Design 11*, had two channels of thickness 1mm each, which fed the scaffold. *Design 11b* had slighter higher shear stress pressure drop values owing to reduction in thickness of the channel. When the results of nutrient distribution in *Design 8* and *Design 11b* were compared, the results of *Design 10b* were better.

5.2 RECOMMANDATION:

1) This study was done using only one cell type. The simulation results should be checked for other cell types too and the effective of designs should be validated.
2) Oxygen solubility is nutrient media is less as compared to other nutrients, so oxygen acts as a limiting reactant in cell culture studies. However, solubility of

oxygen can be increased by increasing the partial pressure inside the nutrient media. For achieving this, oxygen can be bubbled through the media while maintaining the reactor at a pressure higher than atmospheric. Further, simulations should be performed to check the effect of this increased solubility on nutrient distribution.

3) These bioreactor designs have been studied theoretically, and simulations are performed by taking different factors into account. However, these reactors should be built and cell culture should be carried out for the purpose of experimental validation.
4) To see the effect of pressure drop and shear stress on the scaffold and on regenerating tissue, mechanical properties of the scaffold should be incorporated into the simulations.
5) To check the effect of different variables in the simulation, sensitivity analysis needs to done.
6) Using this reactor design it can be predicted that a circular tissue consisting of smooth muscles cells and having diameter of 100mm and 4 mm thickness can be grown. For any further increase in thickness better means of distributing nutrients to growing cells like incorporating blood vessels should be looked into. This can be done by having smart designed scaffolds which would have micro scale capillaries depicting blood vessels.

REFERENCES

Cheng, K., Y. Lai and W. S. Kisaalita (2008). "Three-dimensional polymer scaffolds for high throughput cell-based assay systems." Biomaterials**29**(18): 2802-2812.

Courtney, T., M. S. Sacks, J. Stankus, J. Guan and W. R. Wagner (2006). "Design and analysis of tissue engineering scaffolds that mimic soft tissue mechanical anisotropy." Biomaterials**27**(19): 3631-3638.

Cummings, L. J. and S. L. Waters (2007). "Tissue growth in a rotating bioreactor. Part II: fluid flow and nutrient transport problems." Math Med Biol**24**(2): 169-208.

Devarapalli, M., B. J. Lawrence and S. V. Madihally (2009). "Modeling nutrient consumptions in large flow-through bioreactors for tissue engineering. Biotechnology and Bioengineering." Biotechnology and Bioengineering**103**: 1003-1015.

Freyman, T. M., I. V. Yannas and L. J. Gibson (2001). "Cellular materials as porous scaffolds for tissue engineering." Progress in Materials Science**46**(3-4): 273-282.

Heydarkhan-Hagvall, S., M. Esguerra, G. Helenius, R. Sapderberg, B. R. Johansson and B. Risberg (2006). "Production of Extracellular Matrix Components in Tissue-Engineered Blood Vessels." Tissue Engineering**12**(4): 831-842.

Hollister, S. J. (2005). "Porous scaffold design for tissue engineering." Nature Materials**4**(7): 518-524.

Kim, B. S. and D. J. Mooney (1998). "Development of biocompatible synthetic extracellular matrices for tissue engineering." Trends Biotechnol**16**(5): 224-230.

Liu, C., Z. Xia and J. T. Czernuszka (2007). "Design and Development of Three-Dimensional Scaffolds for Tissue Engineering." Chemical Engineering Research and Design**85**(7): 1051-1064.

Mark Saltzman, W. and S. P. Baldwin (1998). "Materials for protein delivery in tissue engineering." Adv Drug Deliv Rev**33**(1-2): 71-86.

Martin, I., D. Wendt and M. Heberer (2004). "The role of bioreactors in tissue engineering." Trends in Biotechnology**22**(2): 80-86.

Martin, Y. and P. Vermette (2005). "Bioreactors for tissue mass culture: Design, characterization, and recent advances." Biomaterials**26**(35): 7481-7503.

Niklason, L. E., J. Gao, W. M. Abbott, K. K. Hirschi, S. Houser, R. Marini and R. Langer (1999). "Functional Arteries Grown in Vitro." Science**284**(5413): 489-493.

Powell, C. A., B. L. Smiley, J. Mills and H. H. Vandenburgh (2002). "Mechanical stimulation improves tissue-engineered human skeletal muscle." Am J Physiol Cell Physiol(283): C1557 - C1565.

Uygun, B. E., A. Soto-Gutierrez, H. Yagi, M.-L. Izamis, M. A. Guzzardi, C. Shulman, J. Milwid, N. Kobayashi, A. Tilles, F. Berthiaume, M. Hertl, Y. Nahmias, M. L. Yarmush and K. Uygun (2010). "Organ reengineering through development of a transplantable recellularized liver graft using decellularized liver matrix." Nat Med**16**(7): 814-820.

Vance, J., S. Galley, D. F. Liu and S. Donahue (2005). "Mechanical stimulation of MC3T3 osteoblastic cells in a bone tissue-engineering bioreactor enhances prostaglandin E-2 release." Tissue Engineering**11**: 1832-1839.

Yang, S., K. F. Leong, Z. Du and C. K. Chua (2001). "The Design of scaffolds for use in tissue engineering. Part I. Traditional factors." Tissue Engineering**7**(6).

Annabi, N., J. W. Nichol, X. Zhong, C. Ji, S. Koshy, A. Khademhosseinni and F. Dehghani (2010). "Controlling the Porosity and Microarchitecture of Hydrogels for Tissue Engineering." Tissue Engineering**16**(4): 371-383.

Boschetti, F., M. T. Raimondi, F. Migliavacca and G. Dubini (2006). "Prediction of the micro-fluid dynamic environment imposed to three-dimensional engineered cell systems in bioreactors." Journal of Biomechanics**39**(3): 418-425.

Capuani, F., D. Frenkel and C. P. Lowe (2003). "Velocity fluctuations and dispersion in a simple porous medium." Phys Rev E Stat Nonlin Soft Matter Phys**67**(5 Pt 2): 056306.

Chen, H.-C. and Y.-C. Hu (2006). "Bioreactors for tissue engineering." Biotechnology Letters**28**(18): 1415-1423.

Chiu, J. J., S. Usami and S. Chien (2009). "Vascular endothelial responses to altered shear stress: pathologic implications for atherosclerosis. ." Annals of Medicine**41**(1): 19-28.

Chou, T.-C., E. Fu and E.-C. Shen (2003). "Chitosan inhibits prostaglandin E2 formation and cyclooxygenase-2 induction in lipopolysaccharide-treated RAW 264.7

macrophages." Biochemical and Biophysical Research Communications**308**(2): 403-407.

Chung, C. A., C. W. Chen, C. P. Chen and C. S. Tseng (2007). "Enhancement of cell growth in tissueengineering constructs under direct perfusion: Modeling and simulation." Biotechnology and Bioengineering**97**(6): 1603-1616.

Devarapalli, M. (2009). DESIGNING A BIOREACTOR FOR REGENERATING HIGH ASPECT RATIO TISSUES. Master's Thesis.

Gray, M. L., A. M. Pizzanelli, A. J. Grodzinsky and R. C. Lee (1988). "Mechanical and physicochemical determinants of the chondrocyte biosynthetic response." Journal of Orthopaedic Research**6**(6): 777-792.

Griffith, L. G. and G. Naughton (2002). "Tissue engineering--current challenges and expanding opportunities." Science**295**(5557): 5.

Hoerstrup, S. P., R. Sodian, J. S. Sperling, J. P. Vacanti and J. E. J. Mayer (2000). "New pulsatile bioreactor for in vitro formation of tissue engineered heart valves." Tissue-Engineering**6**(1): 75-79.

Hollister, S. J. (2005). "Porous scaffold design for tissue engineering." Nat Mater**4**(7): 518-524.

Holtorf, H. L., T. L. Sheffield, C. G. Ambrose, J. A. Jansen and A. G. Mikos (2005). "Flow perfusion culture of marrow stromal cells seeded on porous biphasic calcium phosphate ceramics." Annals of Biomedical Engineering**33**: 1238-1248.

Huang, Y., S. Onyeri, M. Siewe, A. Moshfeghian and S. V. Madihally (2005). "In vitro characterization of chitosan-gelatin scaffolds for tissue engineering." Biomaterials**26**(36): 7616-7627.

Ishihara, M., K. Obara, S. Nakamura, M. Fujita, K. Masuoka, Y. Kanatani, B. Takase, H. Hattori, Y. Morimoto, M. Ishihara, T. Maehara and M. Kikuchi (2006). "Chitosan hydrogel as a drug delivery carrier to control angiogenesis." J Artif Organs**9**(1): 8-16.

Jaasma, M. J., N. A. Plunkett and F. J. O'Brien (2008). "Design and validation of a dynamic flow perfusion bioreactor for use with compliant tissue engineering scaffolds." Journal of Biotechnology**133**(4): 490-496.

Koller, M. R., S. G. Emerson and B. O. Palsson (1993). "Large-scale expansion of human stem and progenitor cells from bone marrow mononuclear cells in continuous perfusion cultures." Blood**82**(2): 378-384.

Langer, R. and J. P. Vacanti (1993). "Tissue engineering." Science**260**(5110): 920-926.

Lien, S. M., L. Y. Ko and T. J. Huang (2009). "Effect of pore size on ECM secretion and cell growth in gelatin scaffold for articular cartilage tissue engineering." Acta Biomaterialia**5**: 670.

Madihally, S. V. and H. W. T. Matthwe (1999). "Porous chitosan scaffolds for tissue engineering." Biomaterials**20**(12): 1133-1142.

Mandal, B. and S. Kundu (2009). "Cell proliferation and migration in silk fibroin 3D scaffolds." Biomaterials**30**: 2956.

Mao, J., L. Zhao, K. De Yao, Q. Shang, G. Yang and Y. Cao (2003). "Study of novel chitosan-gelatin artificial skin in vitro." J Biomed Mater Res**64A**(2): 301-308.

Martin, I., D. Wendt and M. Heberer (2004). "The role of bioreactors in tissue engineering." Trends in Biotechnology**22**(2): 80-86.

Martin, Y. and P. Vermette (2005). "Bioreactors for tissue mass culture: Design, characterization, and recent advances." Biomaterials**26**(35): 7481-7503.

Moshfeghian, A., J. Tillman and S. V. Madihally (2006). "Characterization of emulsified chitosan-PLGA matrices formed using controlled-rate freezing and lyophilization technique." J Biomed Mater Res A**79**(2): 418-430.

O'Brien, F. J., B. A. Harley, I. V. Yannas and L. Gibson (2004). "Influence of freezing rate on pore structure in freeze-dried collagen-GAG scaffolds." Biomaterials**25**(6): 1077-1086.

Otsuki, B., M. Takemoto, S. Fujibayashi, M. Neo, T. Kokubo and T. Nakamura (2006). "Pore throat size and connectivity determine bone and tissue ingrowth into porous implants: Three-dimensional micro-CT based structural analyses of porous bioactive titanium implants." Biomaterials**27**(35): 5892-5900.

Papadaki, M., S. G. Eskin, J. Ruef, M. S. Runge and L. V. McIntire (1999). "Fluid shear stress as a regulator of gene expression in vascular cells: possible correlations with diabetic abnormalities." Diabetes Research and clinical practice.**45**(2): 89-99.

Porter, B., R. Zauel, H. Stockman, R. Guldberg and D. Fyhrie (2005). "3-D computational modeling of media flow through scaffolds in a perfusion bioreactor." J Biomech**38**(3): 543-549.

Portner, R., S. Nagel-Heyer, C. Goepfert, P. Adamietz and N. M. Meenen (2005). "Bioreactor design for tissue engineering." J Biosci Bioeng**100**(3): 235-245.

Raimondi, M. T., M. Moretti, M. Cioffi, C. Giordano, F. Boschetti, K. Lagana and R. Pietrabissa (2006). "The effect of hydrodynamic shear on 3D engineered chondrocyte systems subject to direct perfusion." Biorheology**43**(3-4): 215-222.

Reich, K. M. and J. A. Frangos (1991). "Effect of flow on prostanglandin E2 and inositol triphosphate levels in osteoblasts." Am J Physiol Cell Physiol**261**(3): C428.

Reignier, J. and M. A. Huneault (2006). "Preparation of interconnected poly([epsilon]-caprolactone) porous scaffolds by a combination of polymer and salt particulate leaching." Polymer**47**(13): 4703-4717.

Risbud, M. V. and M. Sittinger (2002). "Tissue engineering: advances in in vitro cartilage generation." Trends in Biotechnology**20**(8): 351-356.

Shito, M., N. H. Kim, H. Baskaran, A. W. Tilles, R. G. Tompkins, M. L. Yarmush and M. Toner (2001). "In Vitro and In Vivo Evaluation of Albumin Synthesis Rate of Porcine Hepatocytes in a Flat-Plate Bioreactor." Artificial Organs**25**(7): 571-578.

Singh, H. and D. Hutmacher (2009). Bioreactor Studies and Computational Fluid Dynamics. Bioreactor Systems for Tissue Engineering. C. Kasper, M. van Griensven and R. Pörtner, Springer Berlin / Heidelberg. **112:** 231-249.

Takahashi, M. and B. C. Berk (1996). "Mitogen-activated protein kinase (ERK1/2) activation by shear stress and adhesion in endothelial cells." The Journal of clinical Investigation**98**(11): 2623-2631.

Thein-Han, W. W., J. Saikhun, C. Pholpramoo, R. D. K. Misra and Y. Kitiyanant (2009). "Chitosan-gelatin scaffolds for tissue engineering: Physico-chemical properties and biological response of buffalo embryonic stem cells and transfectant of GFP-buffalo embryonic stem cells." Acta Biomaterialia**5**(9): 3453-3466.

Van, T., G. H. Tony, G. J. C. Ralf, P. d. G. Buma, H. Jacqueline, A. J. Pennings and R. P. H. Veth (2002). "Tissue ingrowth and degradation of two biodegradable porous polymers with different porosities and pore sizes." Biomaterials**23**(8): 1731-1738.

Wake, M. C., C. W. J. Patrick and A. G. Mikos (1994). "Pore morphology effects on the fibrovascular tissue growth in porous polymer substrates." Cell Transplant**3**(4): 339-343.

Weigel, T., G. Schinkel and L. Andreas (2006). "Design and preparation of polymeric scaffolds for tissue engineering " Expert Review of Medical Devices**3**(6): 17.

Wendt, D., A. Marsano, M. Jakob, M. Heberer and I. Martin (2003). "Oscillating perfusion of cell suspensions through three-dimensional scaffolds enhances cell seeding efficiency and uniformity." Biotechnology and Bioengineering**84**(2): 205-214.

Whang, K., K. E. Healy, D. R. Ellenz, E. K. Nam, D. C. Tsai, C. H. Thomas, G. Nuber, R. Glorieux, R. Travers and S. M. Sprague (1999). "Engineering bone regeneration with bioabsorbable scaffolds with novel microarchitecture." Tissue Engineering**5**(1): 35-51.

Yang, S., K. F. Leong, Z. Du and C. K. Chua (2001). "The Design of scaffolds for use in tissue engineering. Part I. Traditional factors." Tissue Engineering**7**(6).

Alpert, E., A. Gruzman, H. Totary, N. Kaiser, R. Reich and S. Sasson (2002). "A natural protective mechanism against hyperglycaemia in vascular endothelial and smooth-muscle cells: role of glucose and 12-hydroxyeicosatetraenoic acid." The Bochemical journal**362**(Pt 2): 413-422.

Bancroft, G. N., V. I. Sikavitsas and A. G. Mikos (2003). "Design of a Flow Perfusion Bioreactor System for Bone Tissue-Engineering Aplications." Tissue-Engineering**9**(3): 549-554.

Devarapalli, M. (2009). Designing a bioreactor for egenerating high aspect ratio tissues. Master's Thesis.

Devarapalli, M., B. J. Lawrence and S. V. Madihally (2009). "Modeling nutrient consumptions in large flow-through bioreactors for tissue engineering. Biotechnology and Bioengineering." Biotechnology and Bioengineering**103**: 1003-1015.

Iyer, P. (2009). "BIOPHYSICAL EFFECTS OF MATRICES ON CELLULAR COLONIZATION." Master's Thesis.

Motterlini, R., H. Kerger, C. J. Green, R. M. Winslow and M. Intaglietta (1998). "Depression of endothelial and smooth muscle cell oxygen consumption by endotoxin." Am J Physiol**275**(3 Pt 2): H776-782.

Mueller, S. M., S. Mizuno, L. C. Gerstenfeld and J. Glowacki (1999). "Medium perfusion enhances osteogenesis by murine osteosarcoma
cells in three-dimensional collagen sponges." Journal Of Bone And Mineral Research**12**.

Truskey, G. A., F. Yuan and D. F. Katz (2004). Transport Phenomena in Biological Systems. Upper Saddle River, NJ, Pearson Prentice Hall**:** 317-321.

Leddy, H. A., H. A. Awad and F. Guilak (2004). "Molecular diffusion in tissue-engineered cartilage constructs: Effects of scaffold material, time, and culture conditions." Journal of Biomedical Materials Research Part B: Applied Biomaterials**70B**(2): 397-406.

Mackie, J. S. and P. Meares (1955). "Diffusion in a cation exchanger resin I." Proc. R. Soc**232**(A): 448-495.

Mackie, J. S. and P. Meares (1955). "Diffusion in a cation exchanger resin II." Proc. R. Soc**232**(A): 495-505.

Raghavan, D., B. P. Kropp, H. K. Lin, Y. Zhang, R. Cowan and S. V. Madihally (2005). "Physical characteristics of small intestinal submucosa scaffolds are location-dependent." J Biomed Mater Res A**73A**(1): 90-96.

Sengers, B. G., C. C. van Donkelaar, C. W. Oomens and F. P. Baaijens (2005). "Computational study of culture conditions and nutrient supply in cartilage tissue engineering." Biotechnol Prog**21**(4): 1252-1261.

Zhou, H., S. B. Chen, J. Peng and C.-H. Wang (2010). "A study of effective diffusivity in porous scaffold by Brownian dynamics simulation." Journal of Colloid and Interface Science**342**(2): 620-628.

.

APPENDIX A

DETERMINATION OF DIFFUSIVITY OF GLUCOSE THROUGH CHITON-GELATIN SCAFFOLDS

A 1 Introduction:

It was observed from the simulation results that the diffusivity of nutrients through the porous structure will play an important role in nutrient distribution throughout the scaffold. Diffusivity of nutrients through the scaffold is affected by the porosity of the scaffold. Hence, to quantify the relation between diffusivity of nutrients and porosity of scaffold, diffusion experiments were conducted by using 3 scaffolds of different compositions. The conditions for the experiment are as tabulated in **Table A 1**

Parameter		**value**
Temperature		room temperature (25^0C)
Pressure		atmospheric
Glucose concentration		50gm/L
Chitosan-gelatin Scaffold porosity (%)	1) 0.5%-0.5% (wt/v)	92
	2) 1%-1% (wt/v)	83
	3) 2%-2% (wt/v)	77
Volume of liquid in each chamber		120mL

A.2Experiment:

A.2.1 Procedure:

The setup of the experiment is as shown in the **Figure A.1**. The procedure during the entire experiment is as follows:

1) Hydrated Chitosan-Gelatin scaffold is mounted on one of the chambers. Second chamber is then clamped to the first chamber.

2) Known initial glucose concentration of 120 mL solution and 120 mL DI water were poured in Chamber 1 and Chamber 2, respectively. Both the chambers were kept well mixed using magnetic stirrers. Samples (100 µL) were taken from both the chambers after every 10 minutes for 1hour.

3) The collected samples were diluted to 1:9 ratio in DI water, for preparing them for the glucose analysis using *YSI-2700*Bio-scientific analyzer instrument.

4) The instrument setup consists of a glucose standard solution, a glucose buffer solution, a sampling chamber and a dipper tube. Glucose-oxidase membrane was used in *YSI-2700*Bio-scientific analyzer for determining glucose concentration. The instrument needed to be calibrated every time when turned 'ON'. After calibration, the instrument was setup in automatic mode to pick one from the turntable and evaluate the glucose concentration.

Using the glucose concentrations from various time points, membrane permeability was calculated as described previously (Raghavan et al. 2005). In brief, following equation was used assuming a quasi-steady state approximation

$$ln\left(\frac{C_0-2C_2}{C_0}\right) = -\left(\frac{A_m}{V}P\right)t \qquad \text{(A.1)}$$

whereC_2 is the concentration of the glucose measured at any time t in Chamber 2, C_0 is the initial concentration in Chamber 1, A_m is the membrane area (= 9π/4 cm^2, as the radius of the chamber is 3 cm), V is the volume of each chamber (= 120 mL), and P is the Permeability of the matrix. Then $\ln\left(\frac{C_0-2C_2}{C_0}\right)$ was plotted as a function of time from which the slope (= A_mP/V) was determined using a linear fit. The permeability was calculated using the slope values.

A.2.2 Sample experimentation values:

The samples are analyzed for glucose concentration using *YSI-2700*Bio-scientific analyzer instrument. The values of glucose concentration, for example 1%-1% chitosan-gelatin scaffold, are tabulated as shown **Table A.2**.

Time	C_1 (gm/lit)	C_2 (gm/lit)
0	4.52	0
10	4.51	0.01
20	4.49	0.023
30	4.475	0.041
40	4.44	0.073
50	4.4	0.103
60	4.38	0.131

Table A.2 Glucose concentrations in chamber 1 and chamber 2.

APPENDIX B

METHOD OF PORE AREA MEASUREMENT

This is a quick guide for measuring area of pore area *Sigma Scan Pro5*.

B.1 Pore Characterization:

Assuming we have taken a micrograph at a 10X resolution.

1) Open "Sigma scan pro" software → open the Hemocytometer 10X image → (follow path) Image→ calibrate→ Distance and area.

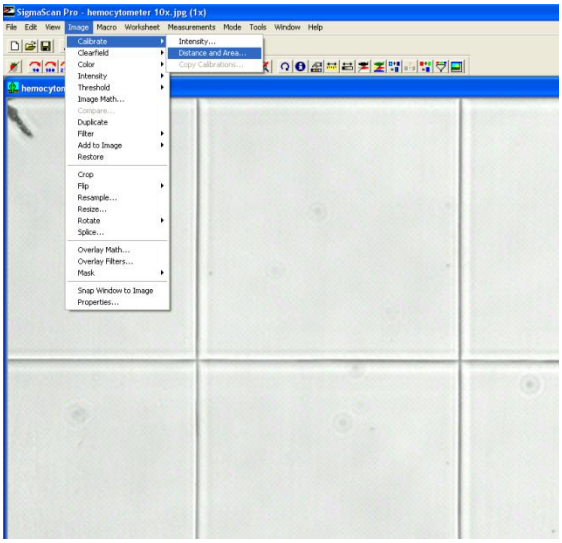

2) A window will pop up. In that window select "2-point calibration". Set old distance=250 and new distance = 388. (or you can set the new distance even by clicking on the adjacent vertices of the hemocytometer square)

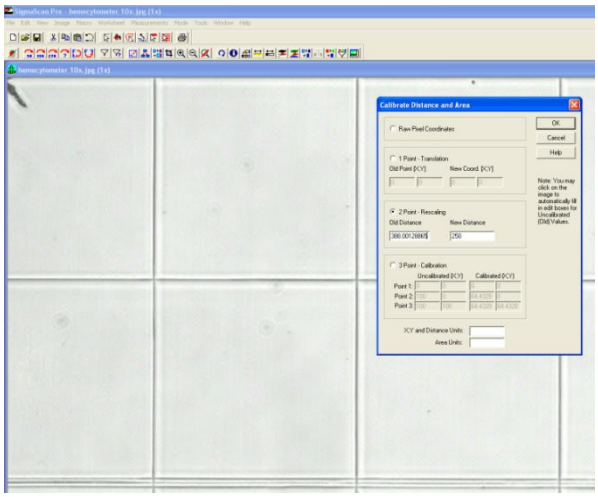

3) Now, without closing the ‘Hemocytometer 10X’ image, open the your correct ‘Micrograph image file’. Go to ‘Image→ Calibrate→ Copy Calibrations…’

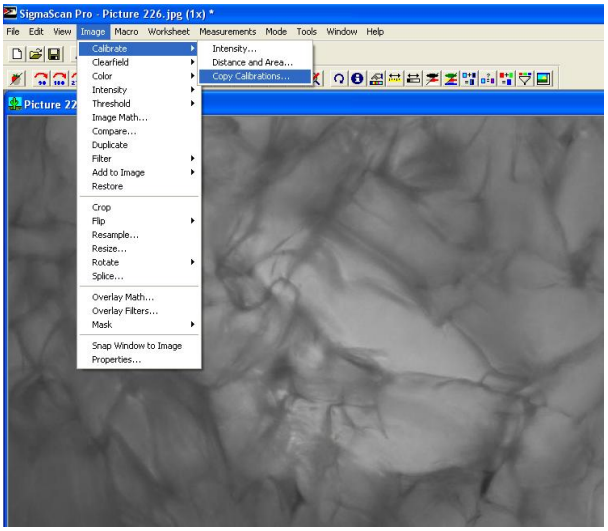

4) A window will pop up. Copy calibrations from ‘Hemocytometer 10X’ to your ‘Micrograph image file’.

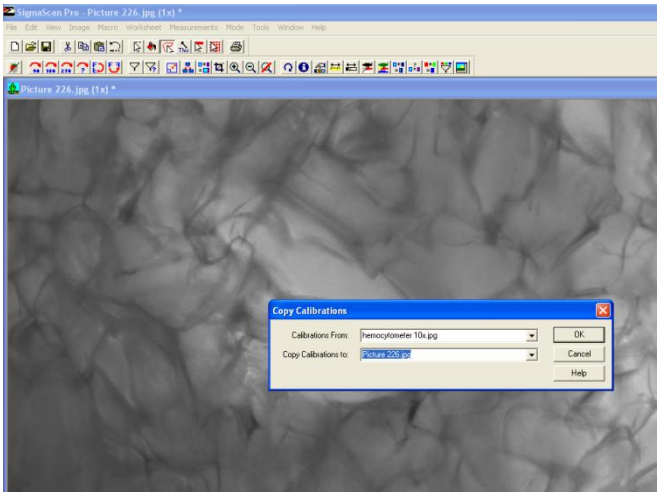

5) Select 'Trace mode→ demarcate the area of the pore by clicking along its perimeter → once you reach your starting point, right click will highlight the area in 'red' color.

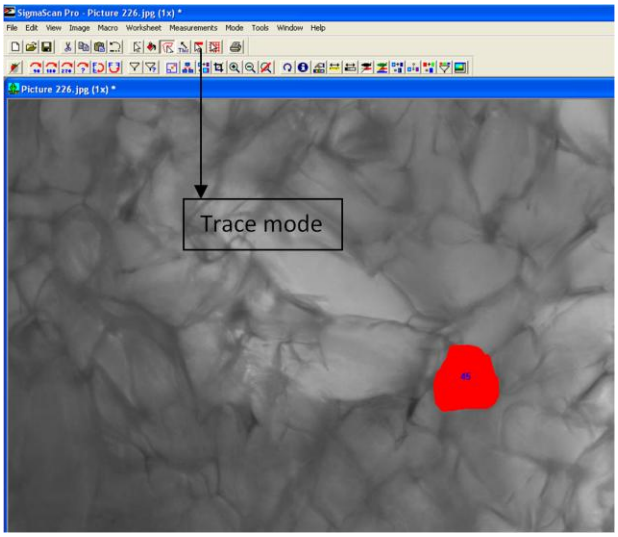

6) Then go to→ Measurements→ Measure objects→ a window will pop up. Click OK.

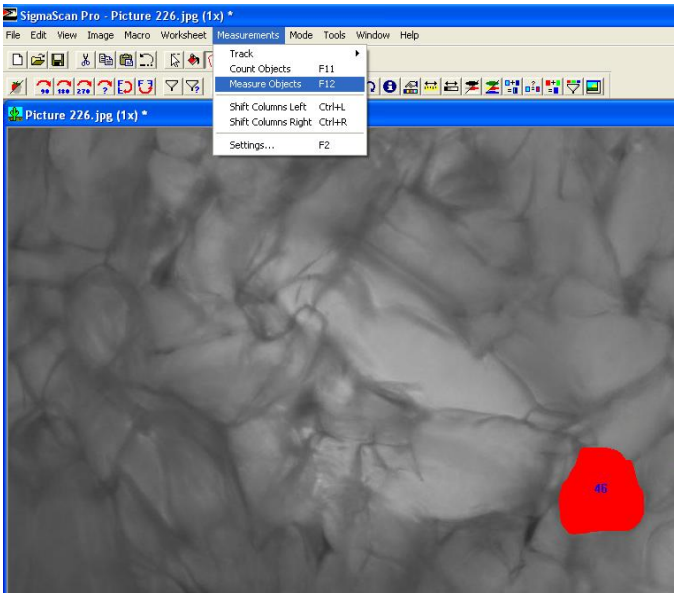

7) You will see an output excel file when you minimize the image window.

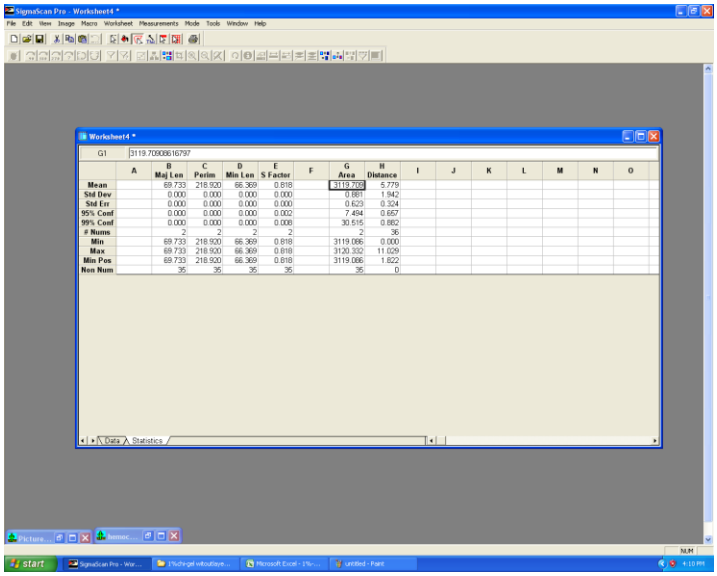

APPENDIX C

COMSOL MANUAL

This is a quick guide to COMSOL Multiphysics 3.5a.

C.1.1 Creating geometry:

1. **Start > All Programs > COMSOL 3.5a >** Click on **COMSOL Multiphysics 3.5a**. Model Navigator window will pop up.

2. In **Model Navigator >**Set **Space Dimension as** 3D

3. In the Application Modes section Click on Chemical Engineering Module >Fluid-Chemical Reactions Interaction>Reacting Flow> Select Steady State Analysis. Click OK. COMSOL Multiphysics Window will pop up.

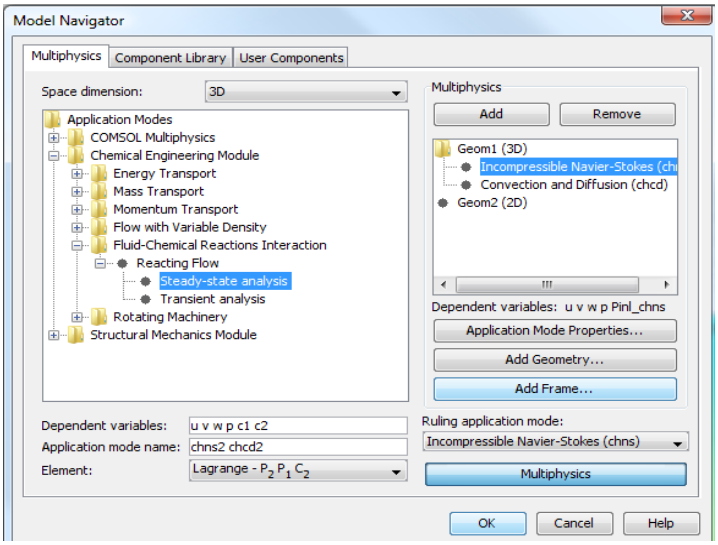

4. Select **Draw** tab > Click on **Work Place Settings**. Work plane settings window will pop up.

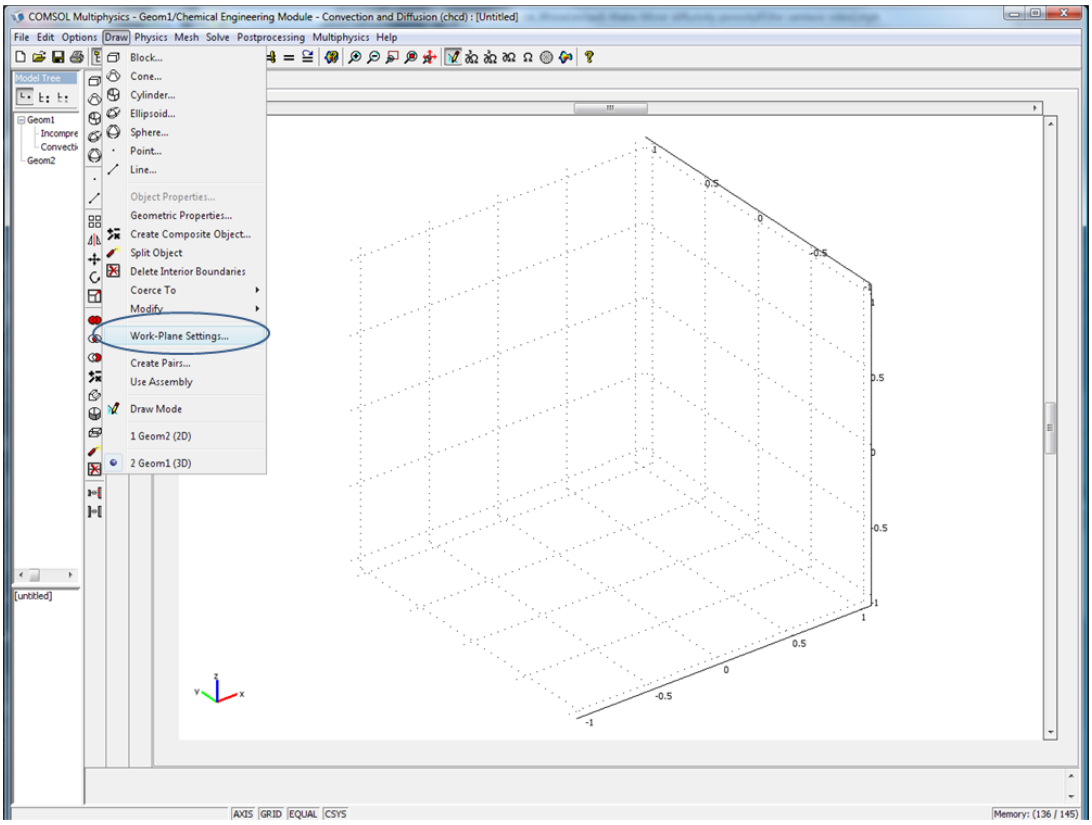

5. Select **Quick** tab > Check on x-y and set z = 0. Click OK.

6. Select **Draw tab> Draw Objects > Click on Ellipse/ Circle (centered)** and create a circle in the Model View. To draw a circle Select a point in the model view and move the mouse to some extent and then click the left button of the mouse once.

7. To Change the dimensions of the object created (say Circle), double click on that particular object a window will pop up. In **Size section>**Change **A semi-axes:** 0.5; Change **B semi-axes:** 0.5. Leave the rest as it is.

8. Click on Geom2 tab in the Model View. Repeat Step 6 and create a circle in the Fourth quadrant (i.e.; quadrant in which both x & y are negative).

9. Repeat Step 7 to Change the dimensions of the circle. In size section > Change A semi-axes: 0.003 and B semi-axes: 0.003. In the Position Section> Change x: -0.028 and y: - 0.028. (This is to create the inlet of 6mm diameter for the circular reactor).

The complete 2D figure can be seen as below.

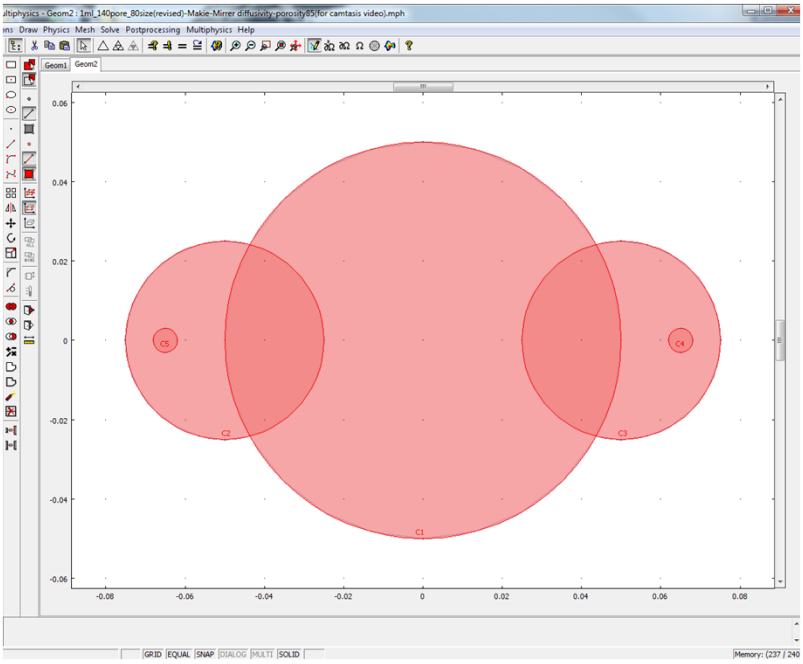

10. To extrude 2D Geometry object to 3D. Select the object that is to be extruded.(In our Case, it is the circle)

11. In the Menu bar Select Draw> Extrude. A window will pop up.

12.In the Extrusion parameters section > Change Distance: 0.002. Leave the rest as it is for Straight Extrusion. Click OK. In the Model View> Geom1 Tab a circle with diameter 10cm and thickness of 2mm will be seen.

13. Repeat Step 9 to extrude. In the Extrusion parameters section > Change Distance: 0.01. Click Ok. In the Model View> Geom1 tab an inlet of 1cm length with a diameter of 6mm is extruded.

14. The circular parallel plate split flow reactor is created.

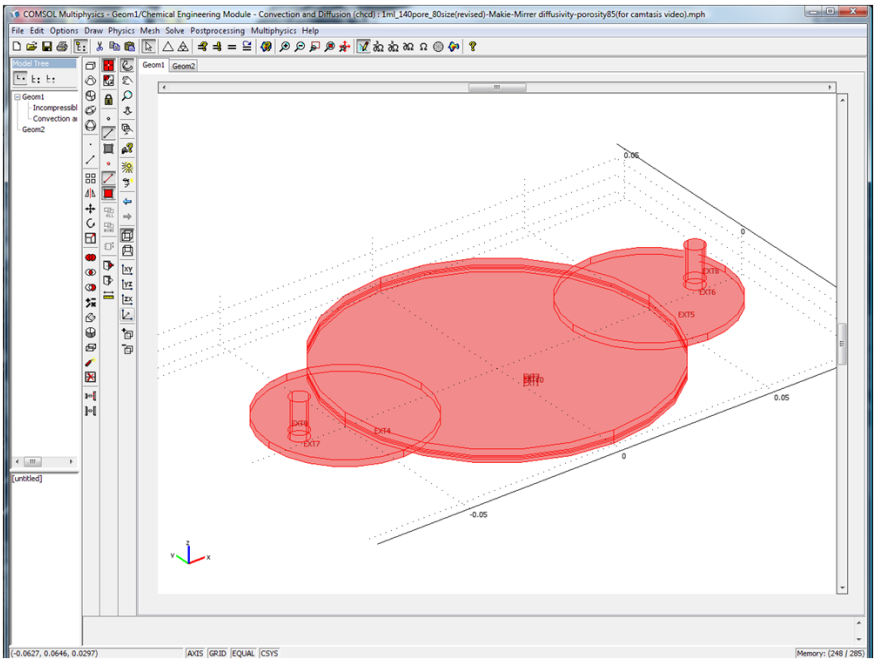

C.1.2 Creating constants list:

Creating a constants list is safe and an easier way to input the parameters which might be used multiple times while writing the boundary conditions.

1. In the Menu bar > Select Options > click on Constants. A window will pop up.

2. In the window that pops up. There will be four columns. Name, Expression, Value and Description. In the Name column type in the name for the parameter. For example, density can be named as rho. In the Expression column enter the values of the constant with units. And then Click Enter the Value will be

automatically shown in the Value column. In the Description column we can write comments for the users to understand about a particular constant.

3. Input the below data in the Constants window that pops up. (the below values are for water flowing through the circular parallel plate split flow reactor having chitosan-gelatin porous structure with 140pores/mm2 , 80um pore size and the volumetric flow rate maintained is 1 mL/min).

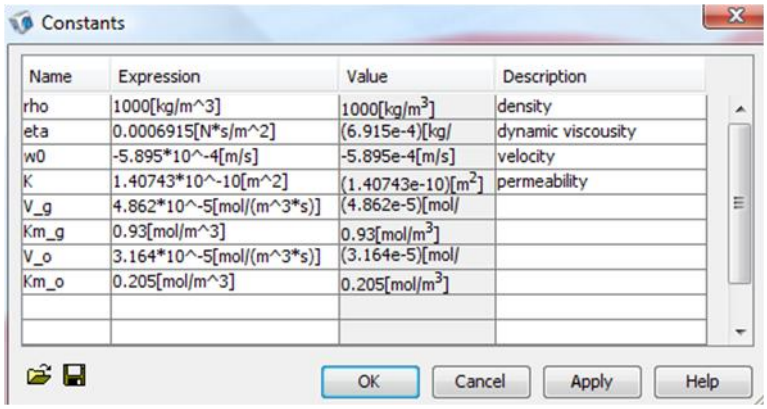

Click OK.

C.1.3 Setting up subdomain and boundary conditions for fluid flow:

C.1.3.1 Subdomain settings:

1. In the Model tree > right click on Incompressible Navier Stokes (chns)> Click on Subdomain Settings. A window will pop up.

2. Select subdomain tab> In the subdomain selection> select all the domains defining fluid filled region in the reactor.

3. Select the physics tab and Input the fluid properties. For ρ: Input the constant *rho*. Similarly for η: input the constant *eta*. Leave the remaining as it is.

4. Next in subdomain selection>select all domains defining porous region in the reactor>Check on the flow in porous media (brinkman equation) option. Input for *k* the constant *K*.

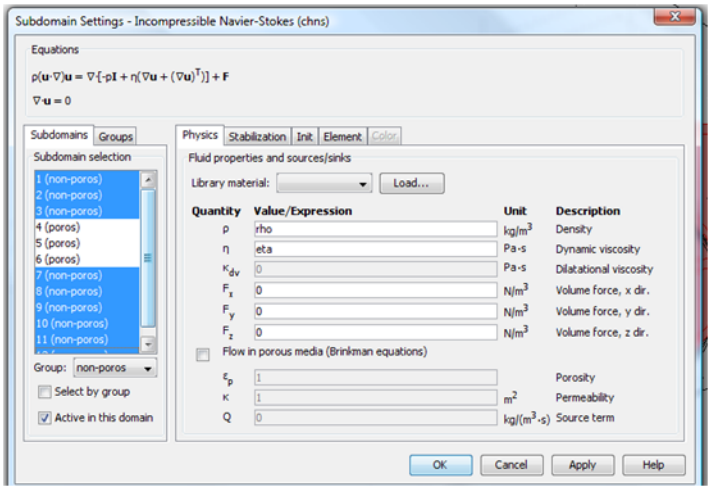

5 Click OK.

C.1.3.2 Boundary settings:

1. In the Model tree > right click on Incompressible Navier Stokes (chns)> Click on Boundary Settings. A window will pop up. In the Boundary tab > Select 11. (it is the inlet Boundary)

2. Select the coefficients tab>Boundary condition: Select velocity. Change w0 value from 0 to w0.

3. In Boundaries tab> select 63 (it is the outlet Boundary)

4. Select the coefficients tab> Boundary condition: select normal flow, pressure. Set P_0 to 0.

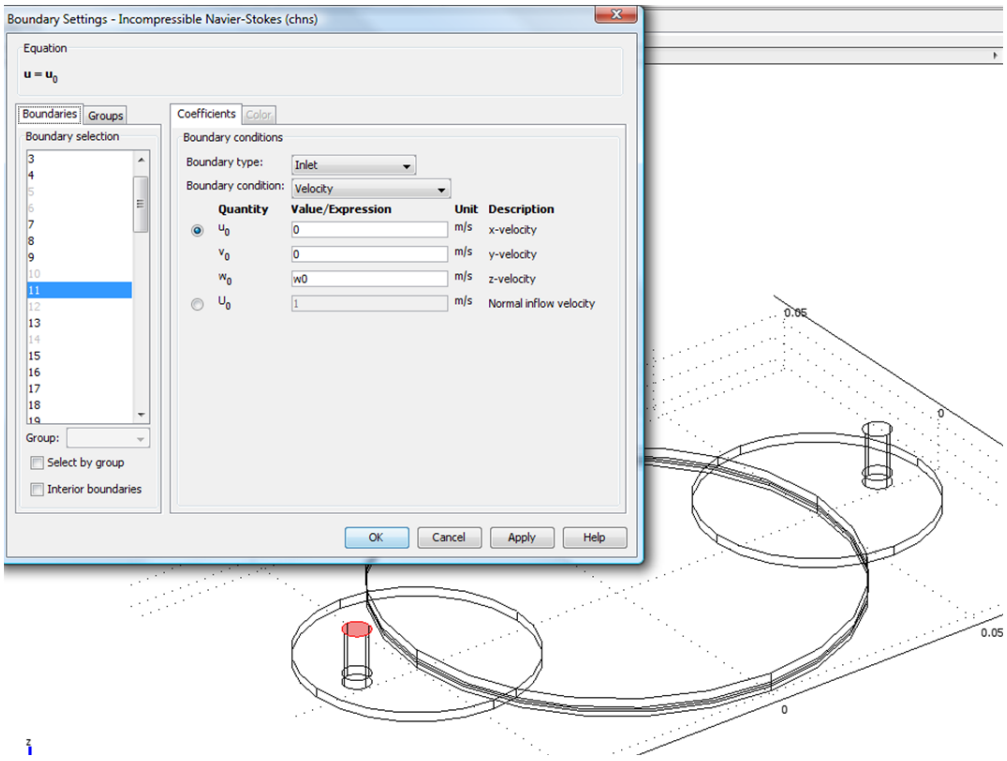

Click OK

C.1.4 Setting subdomain and boundary conditions for reaction:

C.1.4.1 Subdomain settings:

1 In the Model tree > right click on Convection and diffusion (chcd) > Click on Subdomain Settings. A window will pop up.

2. Select subdomain tab > In subdomain selection> select all the domains defining fluid filled region in the reactor.

3. Select c1 >Input the diffusivity value. Similarly input diffusivity value for c2. Set *R* as 0, and u, v and w as u, v and w.

4. Next in subdomain selection>select all domains defining porous region in the reactor>c1>Input reaction rate equation [-V_o*c1/(Km_o+c1)] for R. Similarly for c2, Input reaction rate equation [-V_g*c2/(Km_g+c2)].

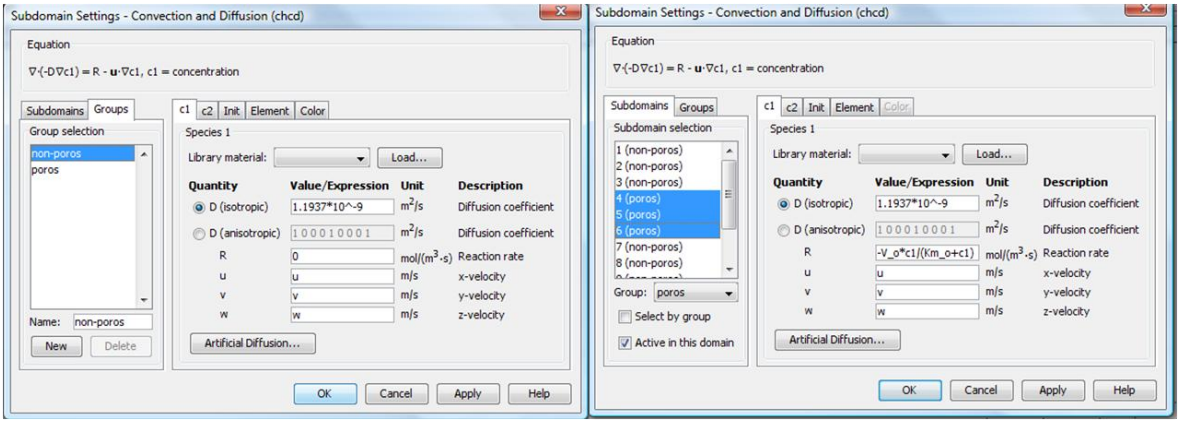

5. Click OK.

C.1.4.2 Boundary settings:

1. In the Model tree > right click on Convection and diffusion (chcd) > Click on Boundary Settings. A window will pop up. In the Boundary tab > Select 11 (it is the inlet Boundary)

2. Select the coefficients tab> Boundary condition: Select Concentration. Input $c1_0$ = 0.199 and $c2_0$ = 5.5.

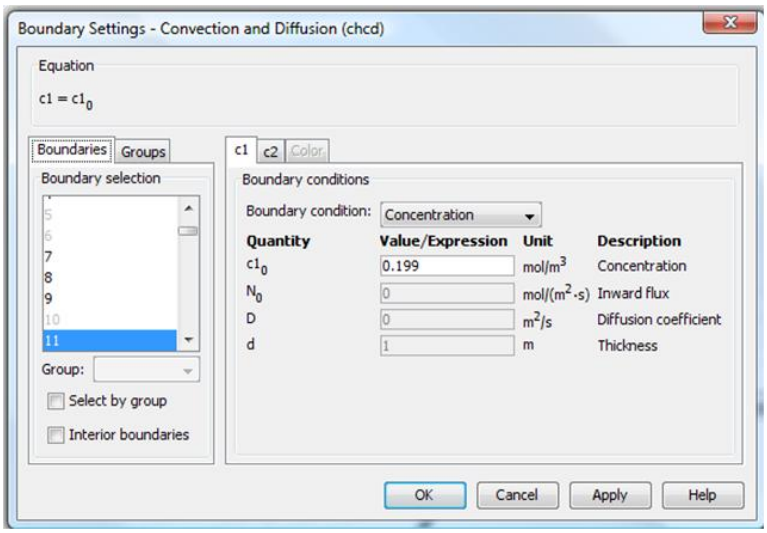

3. In Boundaries tab> select 63 (it is the outlet Boundary)

4. Select the coefficients tab > Boundary condition select convective flux for both c1 and c2.

Click OK

C.1.5 Meshing of the geometry:

1. In the Menu bar > Select Mesh > Free Mesh Parameter. A window will pop up.

2. Select Edge tab > select the edges of input and output > Distribution tab > Under number of edge elements input 3 > click mesh selected.

3. Select Boundary tab > select the boundary 11 and 63 > click mesh selected to mesh those boundaries.

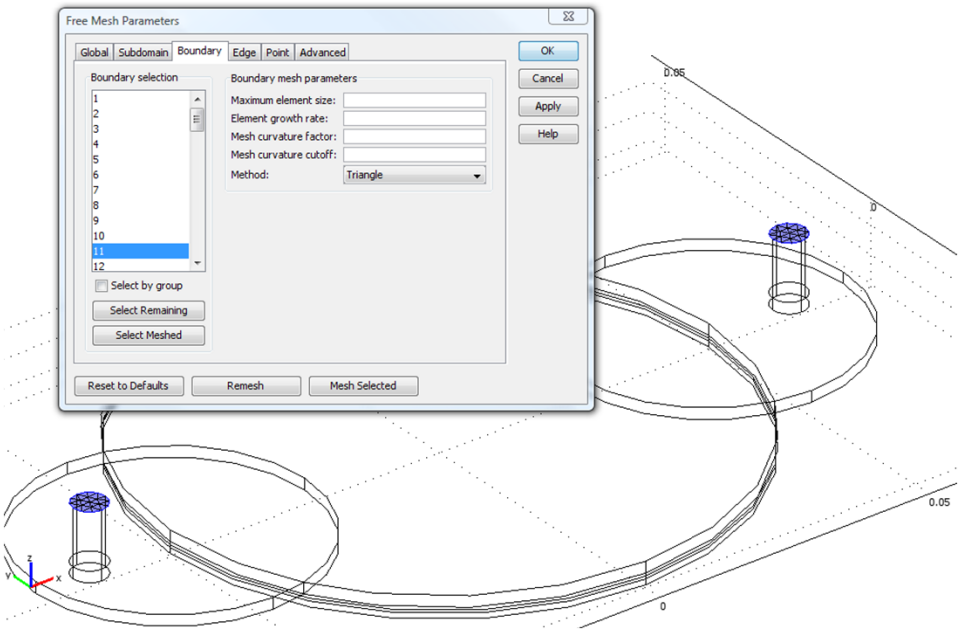

4. Select Mesh tab> swept mesh parameters > select domain 3 and 12 > Elemental layer > check manual specification of elemental layers > 6 > click mesh selected.

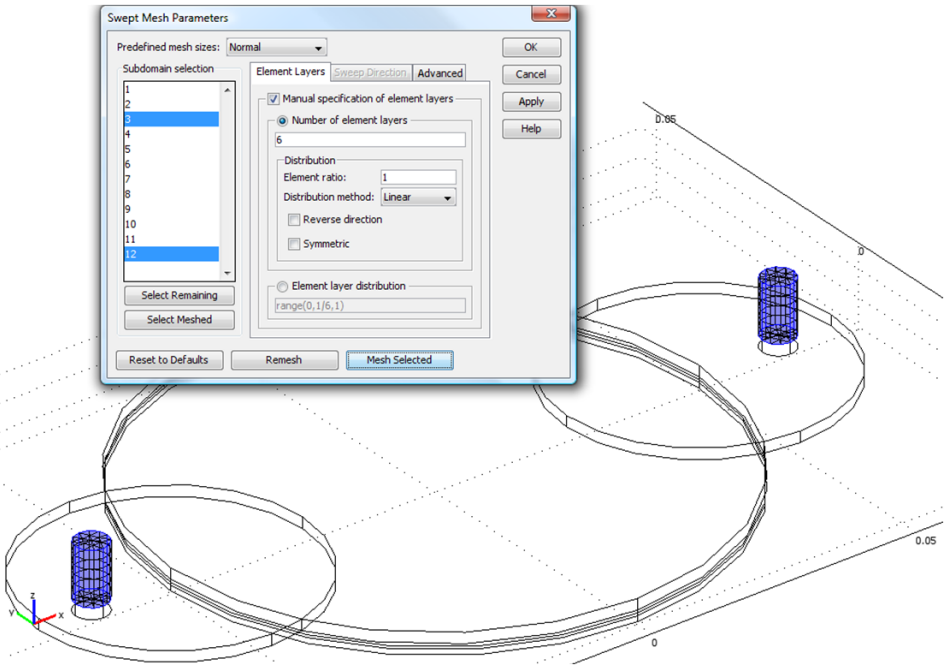

5. Again using Boundary tab in Free mesh parameters, select the topmost boundaries of the reactor > input maximum element size as 0.005 > mesh selected.

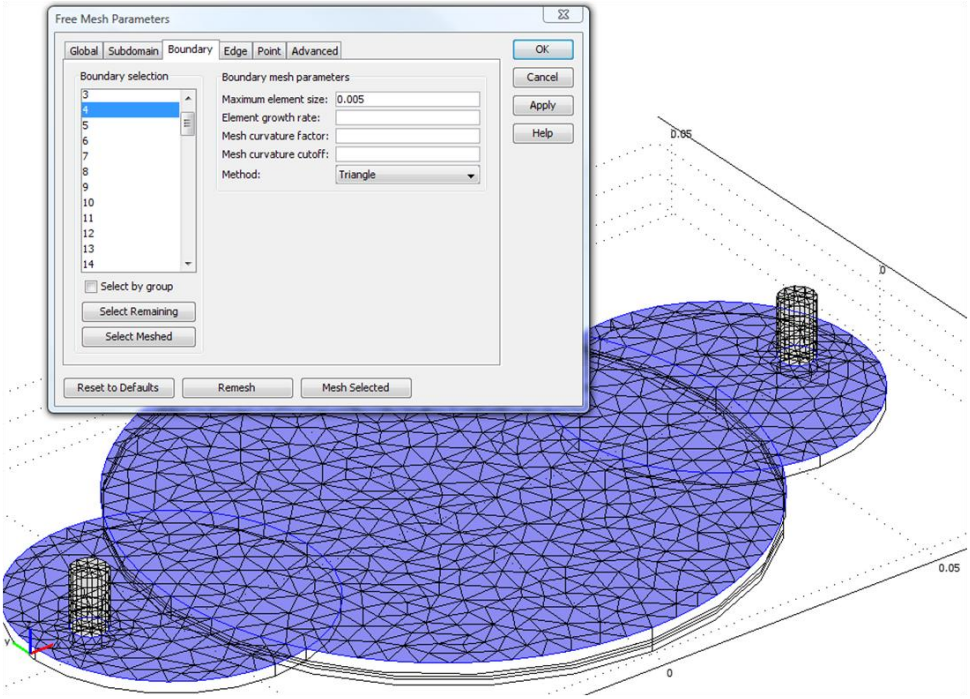

6. Select Mesh tab > swept mesh parameters > select the subdomains particular to the boundaries meshed > Elemental layer > check manual specification of elemental layers > 2 > click mesh selected.

7. Using swept mesh parameters adjacent subdomain > select sweep direction tab > check Manual specification of sweep direction > select source faces and target faces > mesh selected.

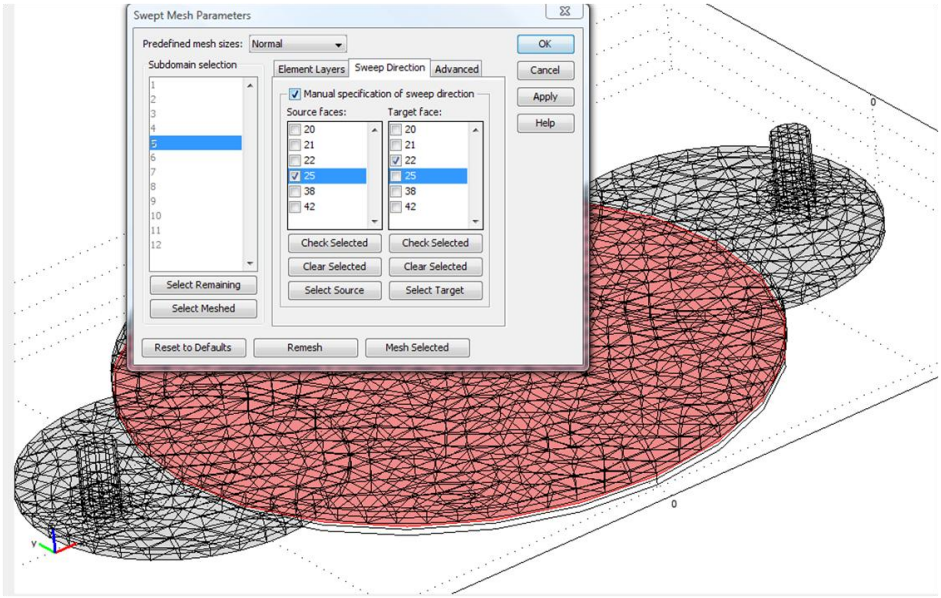

C.1.6Setting up the solver:

1. Go to **Solve** tab in the Menu bar. Click on **Solve Parameters** > A window will popup.

2. In the **Analysis** section select Stationary. Select the **solver** as Stationary.

3. Go to **General** tab >**Linear system solver**: Direct (PARDISO).

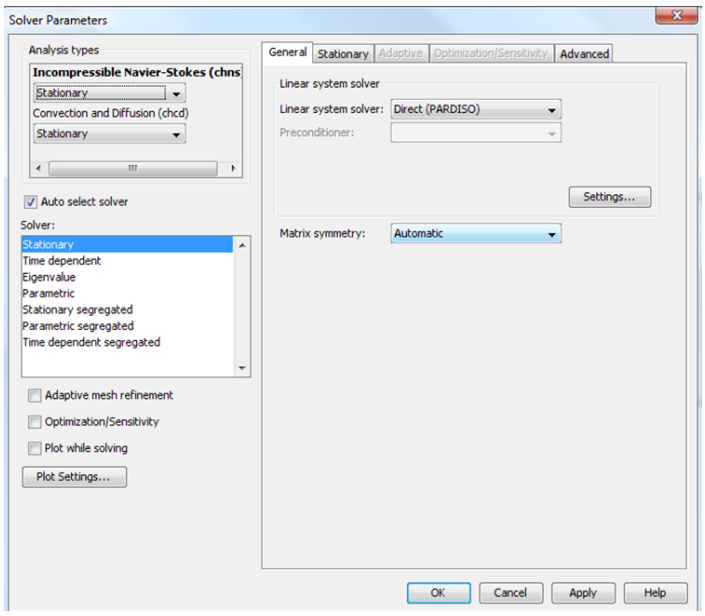

4. Leave the rest as same. Click **OK**.

5. Select the solver according to the requirement.

6. Go to **Solve** tab > Click on **Solver Manager**. A window will pop up.

7. Select **initial value** tab> check mark on **Initial value evaluated using current solution.** In the **Values of variables not solved for and linearization point section** >

   Select **Stored Solution**.

8. Click on **Solve for** tab> Select **Incompressible Navier-Stokes (Chns)**

9. ***Undo*** Select for **Convection and Diffusion** and also ***Und***o select for **Geom2 (2D).**

10. Click **Solve.**

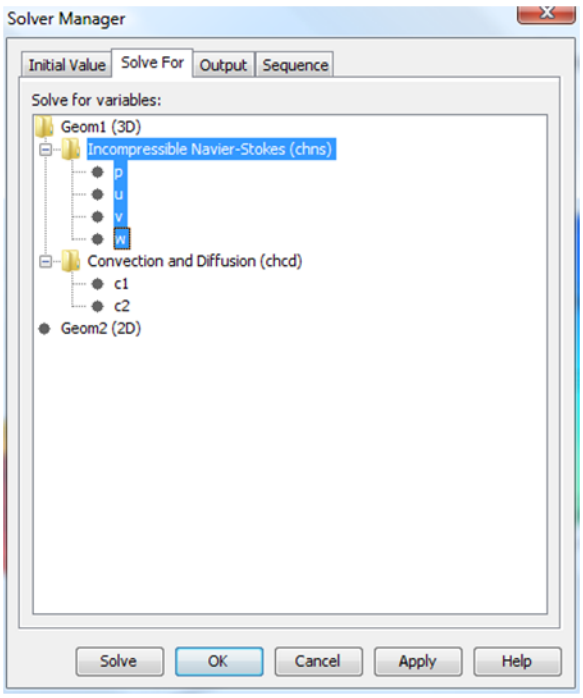

11. After the Solver runs and solves for Navier Stokes equation. Click on **Solve** tab

> **Solver manager**. Select > **Initial value** tab. Click on **stored solution** button. Check on **stored solution**. Select **solve for** tab > select **Convection and diffusion** and

then Click **Solve**.

C.1.7Post processing the results:

1. Go to **Post Processing** tab in the Menu bar> Click on **Plot parameters**. A window

will pop up. Select **Subdomain** tab.

2. **Predefined quantities**> select **Pressure**

3. Click **OK.**

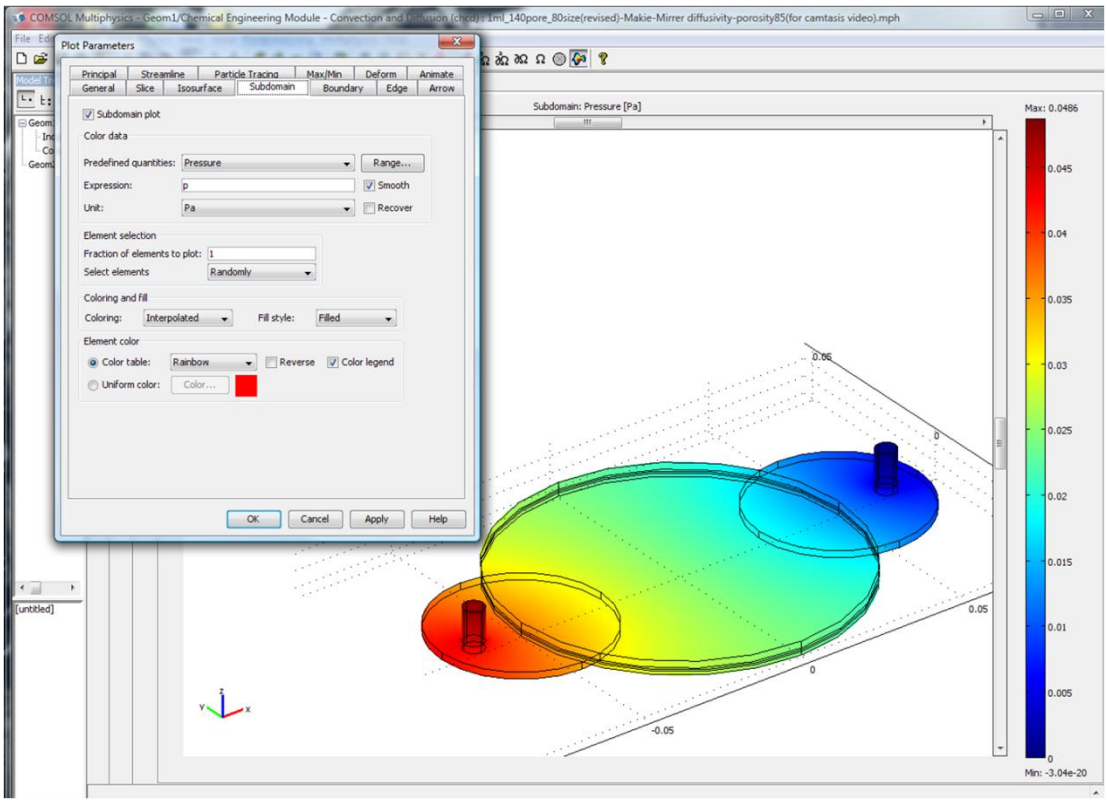
COMSOL Multiphysics - Geom1/Chemical Engineering Module - Convection and Diffusion (chcd) - 1ml_140pore_80size(revised)-Makie-Mirrer diffusivity-porosity85(for camtasis video).mph
Plot Parameters
Principal
Streamline
Particle Tracing
Max/Min
Deform
Animate
General
Slice
Isosurface
Subdomain
Boundary
Edge
Arrow
Subdomain plot
Color data
Predefined quantities:
Pressure
Range...
Expression:
p
Smooth
Unit:
Pa
Recover
Element selection
Fraction of elements to plot:
1
Select elements
Randomly
Coloring and fill
Coloring:
Interpolated
Fill style:
Filled
Element color
Color table:
Rainbow
Reverse
Color legend
Uniform color:
Color...
OK
Cancel
Apply
Help
Subdomain: Pressure [Pa]
Max: 0.0486
0.045
0.04
0.035
0.03
0.025
0.02
0.015
0.01
0.005
0
Min: -3.04e-20
0.05
0
-0.05
[untitled]

VITA

Dhananjay V. Dhane

Candidate for the Degree of

Master of Science

Thesis: INFLUENCE OF DIFFUSION IN TISSUE ENGINEERING BIOREACTORS

Major Field: Chemical Engineering

Biographical:

Education:

Completed the requirements for the Master of Science in Chemical Engineering at Oklahoma State University, Stillwater, Oklahoma in December, 2010.

Completed the requirements for the Bachelor of Science in Petrochemical Engineering at Maharashtra Institute of Technology, Pune University, Pune, Maharashtra, India in May 2005.

Experience:
Process Engineer, Reliance Industries Ltd, India. (2005-2008)

Professional Memberships:
Member of AIChe, 2009

Name: Dhananjay V. Dhane Date of Degree: December, 2010

Institution: Oklahoma State University Location: Stillwater, Oklahoma

Title of Study: INFLUENCE OF DIFFUSION IN TISSUE ENGINEERING BIOREACTORS

Pages in Study: 98 Candidate for the Degree of Master of Science

Major Field: Chemical Engineering:

Scope and Method of Study:

Flow-through reactor configuration has been studied earlier for developing high aspect ratio tissues. However, flow-through configuration is limited by the range of flow rates that can be used. Hence, split channel parallel flow reactor configurations were evaluated. The objective was to minimize the pressure drop and shear stresses values in the bioreactor which can be used for growing tissues having a diameter of 100 mm. Simulations were performed using COMSOL Multiphysics 3.5a. In the new designs, nutrient mass transport through the scaffold was determined to be diffusion dominated. Hence, the effect of diffusivity changes during tissue regeneration was incorporated into the new designs and changes in nutrient transport were further studied. To reduce the effect of diffusivity changes on nutrient sufficiency throughout the reactor, new flow configurations were considered. These new designs were assessed for regeneration of thick scaffolds. New designs were also compared with previous designs for the possibility of regenerating thick tissues.

Findings and Conclusions:

1. New designs with open channel arrangement decreased pressure drop and shear stress values.
2. Depending upon the location of the scaffold, the nutrient transport through the porous structure is governed by convection or diffusion.
3. Nutrient diffusivity through the scaffold is a function of the porosity of the scaffold.
4. Incorporating additional inlets and outlets is necessary to regenerate thicker tissues, dictated by the reduced diffusivities.
5. Maximum thickness of tissue that can be regenerated using the reactor configuration in this study is limited to 4mm.

ADVISER'S APPROVAL: Dr. Sundararajan V. Madihally